Forest fire plumes over the North Atlantic: p-TOMCAT model simulations with aircraft and satellite measurements from the ITOP/ICARTT campaign

Peter A. Cook,[1] Nicholas H. Savage,[1,2,3] Solène Turquety,[4,5] Glenn D. Carver,[1,2] Fiona M. O'Connor,[1,3] Andreas Heckel,[6] David Stewart,[7] Lisa K. Whalley,[8] Alex E. Parker,[9] Hans Schlager,[10] Hanwant B. Singh,[11] Melody A. Avery,[12] Glen W. Sachse,[12] William Brune,[13] Andreas Richter,[6] John P. Burrows,[6] Ruth Purvis,[14] Alastair C. Lewis,[15] Claire E. Reeves,[7] Paul S. Monks,[9] James G. Levine,[1] and John A. Pyle[1,2]

Received 26 May 2006; revised 2 October 2006; accepted 13 December 2006; published 25 April 2007.

[1] Intercontinental Transport of Ozone and Precursors (ITOP) (part of International Consortium for Atmospheric Research on Transport and Transformation (ICARTT)) was an intense research effort to measure long-range transport of pollution across the North Atlantic and its impact on O_3 production. During the aircraft campaign plumes were encountered containing large concentrations of CO plus other tracers and aerosols from forest fires in Alaska and Canada. A chemical transport model, p-TOMCAT, and new biomass burning emissions inventories are used to study the emissions long-range transport and their impact on the troposphere O_3 budget. The fire plume structure is modeled well over long distances until it encounters convection over Europe. The CO values within the simulated plumes closely match aircraft measurements near North America and over the Atlantic and have good agreement with MOPITT CO data. O_3 and NO_x values were initially too great in the model plumes. However, by including additional vertical mixing of O_3 above the fires, and using a lower NO_2/CO emission ratio (0.008) for boreal fires, O_3 concentrations are reduced closer to aircraft measurements, with NO_2 closer to SCIAMACHY data. Too little PAN is produced within the simulated plumes, and our VOC scheme's simplicity may be another reason for O_3 and NO_x model-data discrepancies. In the p-TOMCAT simulations the fire emissions lead to increased tropospheric O_3 over North America, the north Atlantic and western Europe from photochemical production and transport. The increased O_3 over the Northern Hemisphere in the simulations reaches a peak in July 2004 in the range 2.0 to 6.2 Tg over a baseline of about 150 Tg.

Citation: Cook, P. A., et al. (2007), Forest fire plumes over the North Atlantic: p-TOMCAT model simulations with aircraft and satellite measurements from the ITOP/ICARTT campaign, *J. Geophys. Res.*, *112*, D10S43, doi:10.1029/2006JD007563.

1. Introduction

[2] In recent years a number of campaigns have studied the long-range transport of air pollution and its impact on O_3 production, including North Atlantic Regional Experiment (NARE) and Oxidizing Capacity of the Tropospheric Atmosphere (OCTA) in 1993 [e.g., *Wild et al.*, 1996]. The transpacific transport of pollution, including boreal (sub-Arctic) fire emissions, was examined in the Intercontinental Transport and Chemical Transformation (ITCT) 2002, Photochemical Ozone Budget of the Eastern North Pacific

[1]Centre for Atmospheric Science, Department of Chemistry, University of Cambridge, Cambridge, UK.
[2]Atmospheric Chemistry Modelling Support Unit, National Environment Research Council Centres for Atmospheric Sciences, University of Cambridge, Cambridge, UK.
[3]Now at Met Office, Exeter, UK.
[4]Atmospheric Chemistry Modeling Group, Harvard University, Cambridge, Massachusetts, USA.
[5]Now at Service d'Aéronomie, Institut Pierre-Simon Laplace, Paris, France.
[6]Institute of Environmental Physics, University of Bremen, Bremen, Germany.
[7]School of Environmental Sciences, University of East Anglia, Norwich, UK.
[8]School of Chemistry, University of Leeds, Leeds, UK.
[9]Department of Chemistry, University of Leicester, Leicester, UK.
[10]Institut fuer Physik der Atmosphaere, Deutsches Zentrum fuer Luft- und Raumfahrt, Oberpfaffenhofen, Germany.
[11]NASA Ames Research Center, Moffett Field, California, USA.
[12]NASA Langley Research Center, Hampton, Virginia, USA.
[13]Department of Meteorology, Pennsylvania State University, University Park, Pennsylvania, USA.
[14]Facility of Airborne Atmospheric Measurements, Cranfield, UK.
[15]Department of Chemistry, University of York, York, UK.

0148-0227/07/2006JD007563

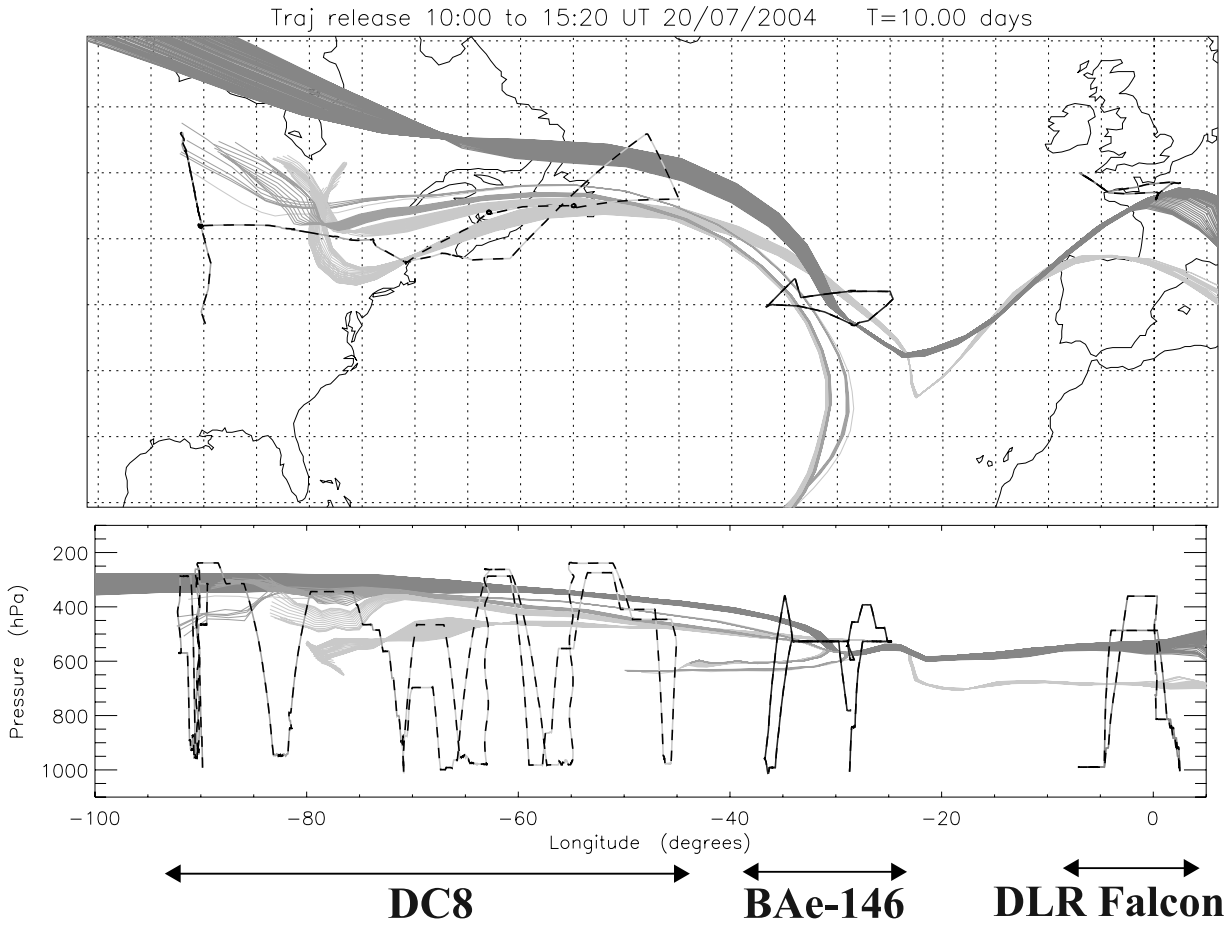

Figure 1. The 3-D trajectory of the large fire plume over several days (dark lines, the lighter lines are trajectories of air masses potentially containing anthropogenic pollution), intercepted by the DC8 over the eastern USA on 18 July 2004, by the BAe-146 in the mid-Atlantic on 20 July and by the DLR Falcon over western Europe on 23 July. The locations of the three flight tracks are shown by the dashed lines. The panels are reproduced from *Methven et al.* [2006].

Atmosphere (PHOBEA) and Pacific Exploration of Asian Continental Emission (PEACE-B) campaigns [e.g., *Bertschi et al.*, 2004; *Hudman et al.*, 2004]. Intercontinental transport of pollution remains a major research theme. In this context International Consortium for Atmospheric Research on Transport and Transformation (ICARTT) was a large international project involving groups from the USA, Canada, France, Germany, the UK and Portugal. It was composed of smaller national projects including Intercontinental Transport of Ozone and Precursors (ITOP), Intercontinental Chemical Transport Experiment–North America (INTEX-NA), ITCT-2K4 and New England Air Quality Study (NEAQS). The aim was to study the long-range influence of pollutants (such as CO and NO_x) from North America, and the production and transport of O_3 in the troposphere. A variety of atmospheric measurements were made over North America, the North Atlantic and Europe during intensive field campaigns between June and August 2004, including remote sensing from satellite instruments (for further details see the overview of ICARTT by *Fehsenfeld et al.* [2006]). ICARTT used research aircraft to make in situ measurements of a range of trace gases in July and August 2004. The NASA DC8 aircraft and the NOAA P3 aircraft flew from the US east coast (part of INTEX-NA), while the UK BAe-146 research aircraft was based in the Azores and the DLR Falcon aircraft was based at Creil, France (part of ITOP).

[3] Central to the observational strategy of ICARTT were attempts to observe the same air mass over several days using the different aircraft in order to measure the chemical aging of polluted air. In an earlier study *Methven et al.* [2003] used the Reverse Domain Filling (RDF) method to follow the trajectories of air masses over the North Atlantic and match flight data to particular air masses by their equivalent potential temperature and specific humidity. Here by using back trajectories *Methven et al.* [2006] identified those air masses which were intercepted by two or more flights during the ICARTT campaign.

[4] The primary objective of the project was to observe long-range transport of anthropogenic pollution from North America and Figure 1 shows in the light bands the 3-D trajectories of air masses, believed to originate from close to emission regions for anthropogenic pollution, and their advection across the Atlantic. Aircraft flight tracks for several flights in July, which were designed to intercept the air parcels, are also shown. However, during the campaign the aircraft also encountered plumes from huge forest fires which burned in Alaska and west Canada

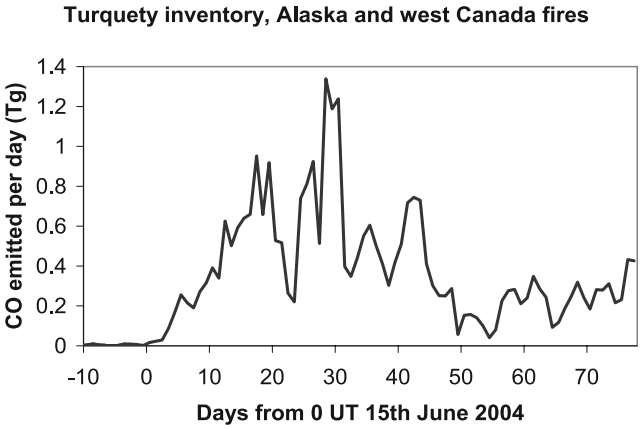

Figure 2. Emission of CO (Tg day^{-1}) from the Alaskan and west Canadian fires during June to August 2004, from the *Turquety et al.* [2007] daily inventories of biomass burning.

between June and September 2004 emitting large quantities of CO and other species (see IGAC Newsletter, issue 32, November 2005). An especially intense fire plume was measured by the DC8 over the eastern USA on 18 July, by the BAe-146 over the mid-Atlantic on 20 July (when CO was measured at over 500 ppbv and a brown haze was visible), and then by the DLR Falcon over western Europe on 23 July. Figure 1 also shows the 3-D trajectories originating in the midtroposphere above the location of the fires, indicating that these air parcels too should have been sampled by the aircraft. *Real et al.* [2007] have used observations from these three flights with a photochemical trajectory model to examine the chemical evolution of the intense fire plume. In contrast, our approach here is to use a chemistry transport model.

[5] Biomass burning is a major source of trace gases in the troposphere but is highly variable in space and time and so is a significant factor in the interannual variability of atmospheric composition. Each year forest fires in many regions of the world emit 171–561 Tg of CO, 2.4–5.0 Tg N of NO_2 and a variety of other gases and aerosols (M. G. Schultz et al., Global emissions from vegetation fires from 1960 to 2000, submitted to *Global Biogeochemical Cycles*, 2006). Biomass burning emissions can travel thousands of kilometers and cover extensive regions, especially when the heat from the fires creates pyroconvective plumes that can reach the upper troposphere and lower stratosphere [*Fromm et al.*, 2005]. In the presence of NO_x and OH, CO can be a major precursor of O_3 production, so that biomass burning, with high levels of these gases, could have a large impact on tropospheric pollution, and O_3 budgets, over large regions, leading to enhanced CO and O_3 at the surface a long distance downwind of the burning regions.

[6] Individual biomass burning events can be very large. One of the greatest of the twentieth century was associated with the Indonesian wildfires of September to November 1997 with estimated emissions of 124 Tg of CO and 2.6 Tg N of NO_2 [*Duncan et al.*, 2003a]. Model results including the fire emissions better reproduce observed CO over the Seychelles, Australia and Hawaii, and observed O_3 over Java, Samoa and Tahiti [*Duncan et al.*, 2003b]. *Chandra et al.* [2002] examined observed tropospheric column ozone over the tropics, 15°S to 15°N, during September and October 1997 and using the GEOS-CHEM global tropospheric chemistry model found a net increase of 6–8 Tg over a climatological mean of 77 Tg. The results suggested that most of the increase in ozone was caused by the biomass burning in Indonesia. *Aghedo et al.* [2006] used a coupled global chemistry climate model MOZECH to examine the importance of African biomass burning to tropospheric ozone budgets and estimated mean annual increases of 2.4 Tg over Africa and 9 Tg globally (about 2–3% of the global tropospheric ozone burden).

[7] Boreal (sub-Arctic) fire emissions were examined by *Wofsy et al.* [1992], *Wotawa and Trainer* [2000] and *McKeen et al.* [2002]. *Wotawa and Trainer* [2000] estimated that Canadian forest fires emitted 12 Tg of CO between mid-June to mid-July 1995, exceeding the total anthropogenic CO emissions for North America during this period by a factor of 2. *Wofsy et al.* [1992] examined aircraft measurements of haze in the sub-Arctic caused by wildfires, finding a mean NO_y/CO ratio of 0.0056 (where a least a third of the NO_y was in the form of PAN and most of the rest was nitrate), rapid conversion of NO_x to reservoir species due to high concentrations of reactive hydrocarbons in smoke plumes, and $\Delta O_3/\Delta CO$ enhancement ratios of only 0.1 compared to 0.3–0.5 for midlatitude pollution. *McKeen et al.* [2002] estimated a NO_2/CO emission ratio of 0.007 for boreal fires based on model simulations of O_3 production combined with measured NO_y. In contrast, lower-latitude fire estimates have a higher NO_2/CO emission ratio (e.g., 0.042 for the Indonesian fires from *Duncan et al.* [2003a]). To assess the global impact of fires, it is clearly necessary to understand the nature and magnitude of the major emissions. In particular it is important to use observations to evaluate inventories of the NO_2 emissions from high-latitude fires.

[8] This paper seeks to investigate whether the fires in Alaska in 2004 were only of regional importance or had an impact on a wider, even hemispheric scale. The global chemistry transport model p-TOMCAT was run with new daily inventories of biomass burning emissions [*Turquety et al.*, 2007], in which the Alaskan and west Canadian forest fires emitted 27 Tg of CO, (which includes 9 Tg of CO from peat burning), and 0.5 Tg N of NO_2 during June to August 2004. Figure 2 shows the daily emissions of CO from these fires in the new inventories, with the largest peak (up to 1.34 Tg of CO day^{-1}) in mid-July responsible for the intense fire plume measured by the aircraft (Figure 1). The new inventories giving a total of 27 Tg of CO are in good agreement with *Pfister et al.* [2005] who used satellite observations in a top-down inverse analysis to optimize the CO emissions from the fires, finding a best estimate of 30 ± 5 Tg. This inventory in the chemical transport model allows us to simulate the fire plume locations and the concentrations of CO and other trace gases. We examine the changes in atmospheric composition resulting from the forest fires in Alaska and west Canada, including the impact on O_3 production in the troposphere and pollution and O_3 levels over North America, the North Atlantic and Europe.

[9] Section 2 describes the aircraft observations and the satellite instrument data. Section 3 describes p-TOMCAT, the inventories of the biomass burning emissions, and the

four model simulations used (a control integration without the fire emissions over Alaska and western Canada; a run including the fire emissions and a simplified treatment of their pyroconvective lifting; a run also including a simplified pyroconvective mixing of O_3 over the fires; and a fourth integration with a reduction in the NO_2/CO ratio for the fire emissions to examine the sensitivity of the model chemistry). Section 4.1 compares the modeled CO to satellite and aircraft measurements to examine the model transport. Section 4.2 compares the modeled O_3, NO_x, PAN and HO_2 to measurements to examine the chemistry in the plumes. Section 4.3 uses the model simulations to examine the impact of the fire emissions on global and regional tropospheric O_3, while section 4.4 examines enhancements in surface CO and O_3 over the UK. Conclusions are drawn in section 5.

2. Observations

2.1. Aircraft Observations

[10] The aircraft provided extensive measurements of a wide variety of trace gases. In this study we use measurements of CO, O_3, NO, PAN and peroxy radicals (HO_2+RO_2) from the BAe-146, measurements of CO, O_3, NO, PAN, NO_2, HNO_3 and HO_2 from the DC8, and measurements of CO, O_3, NO and NO_y from the DLR Falcon.

[11] On the BAe-146, CO was measured using an aerolaser UV monitor with 10s integration and 2 ppbv detection limit [*Gerbig et al.*, 1999] and O_3 by a thermo environmental (TECO 49) UV photometric instrument. NO was measured by chemiluminescence with in-flight sensitivity checks using a standard concentration of NO [*Brough et al.*, 2003] and PAN by using a custom built gas chromatograph with electron capture detection (GC-ECD) with 90s integration, 5 pptv detection limit and preflight calibration [*Whalley et al.*, 2004)]. HO_2 + RO_2 was measured using a peroxy radical chemical amplifier (PERCA) [*Green et al.*, 2006; A. E. Parker et al., Peroxy radicals and ozone photochemistry in air masses undergoing long-range transport, submitted to *Journal of Geophysical Research*, 2006].

[12] On the DC8, NO_2 was measured using laser induced fluorescence (LIF) with a detection sensitivity of 0.8 ppt/min at S/N = 2 and an uncertainty in the instrument zero of less than 1 ppt [*Cleary et al.*, 2002]. All the instruments on the DC8 are described by *Singh et al.* [2006].

[13] On the DLR Falcon, CO was measured with an upgraded aerolaser vacuum UV fluorescence instrument [*Gerbig et al.*, 1999] with a time integration of 5s and an accuracy of 5%. O_3 was measured with a UV absorption technique (Thermo Electron TE49) also with 5s time integration and 5% accuracy. The measurement of NO and NO_y was based on a NO-O_3-chemiluminscence technique [*Schlager et al.*, 1999], 1s time integration with accuracy of 7% (NO) and 12% (NO_y). In the NO_y measurement channel reactive nitrogen species were reduced to NO before detection using a heated gold converter.

2.2. Satellite Data

[14] Profiles of CO in the troposphere were measured remotely by the MOPITT (Measurement Of Pollution In The Troposphere) instrument on the EOS-Aura satellite [*Drummond and Mand*, 1996; *Edwards et al.*, 1999]. This data is available to download from the Web site of the NCAR MOPITT Team. Satellite remote sensing measurements of a wide range of trace gases were made by the SCIAMACHY (Scanning Imaging Absorption Spectrometer for Atmospheric Chartography) instrument [*Bovensmann et al.*, 1999] on the ENVISAT satellite during the campaign period. SCIAMACHY is a passive remote sensing instrument measuring backscattered Earth radiance and extraterrestrial irradiance in the UV, visible and near IR wavelength range. The NO_2 retrieval is based on a DOAS fit using the spectral window from 425 nm to 450 nm [*Richter and Burrows*, 2002]. The stratospheric part of the column was removed by the reference sector method: measurements from the Pacific sector (170–210°E) are assumed to have no tropospheric NO_2 and are subtracted from the other measurements in each latitude. Only pixels with a cloud cover less than 10% were used. A more detailed description regarding the air mass factors applied in the retrieval is given by *Richter et al.* [2005].

3. The p-TOMCAT Model

3.1. Model Description

[15] The model used in this study is the global chemistry and transport model p-TOMCAT driven by specified meteorological fields. It is an updated version [see *O'Connor et al.*, 2005] of a model previously used for a range of tropospheric chemistry studies [*Law et al.*, 1998, 2000; *Savage et al.*, 2004]. Tracer advection was calculated with the second-order moments advection scheme of *Prather* [1986] as implemented by *Chipperfield et al.* [1996] with a 30 min time step. Convective transport was based on the mass flux parameterization of *Tiedke* [1989]. The parameterization includes parameterized deep and shallow convection with convective updrafts and large-scale subsidence, as well as turbulent and organized entrainment and detrainment. The model contains a nonlocal vertical diffusion scheme based on the parameterization of *Holtslag and Boville* [1993]; for details of the scheme implementation see *Wang et al.* [1999].

[16] In this study p-TOMCAT was run with a 2.8° × 2.8° horizontal resolution and 31 vertical levels from the surface to 10 hPa. The offline meteorological fields used are from the operational analyses of the European Medium Range Weather Forecast model, updated every 6 hours. The model represents the transport and chemistry of 42 chemical compounds including tracers of stratospheric ozone and nitrogen oxides, of which 32 tracers are advected. The chemical mechanism includes the chemistry of methane, ethane and propane plus their oxidation products and includes 89 bimolecular, 16 termolecular and 27 photolysis reactions. The version of the chemistry scheme used here did not include isoprene, higher alkanes, alkenes or aromatics. Implications of this are discussed in section 4.2. The model chemistry uses the atmospheric chemistry integration package ASAD [*Carver et al.*, 1997] and is integrated with the IMPACT scheme of *Carver and Stott* [2000]. The ozone and nitrogen oxide concentrations at the top model level are constrained to zonal mean values calculated by the Cambridge 2-D model [*Law and Nisbet*, 1996]. The chemical rate coefficients used by p-TOMCAT have been recently updated to those in the IUPAC Summary of March 2005 (see the Web site http://www.iupac-kinetic.ch.cam.ac.uk).

Table 1. Four Model Simulations

Simulation	Description
A	no biomass burning (BB) emissions from Alaska and west Canada
B	Alaska and west Canada BB emissions put in between surface and ~250 hPa
C	BB emissions + "pyroconvective" vertical mixing of O_3 over Alaska and west Canada
D	reduced NO_2 BB emissions + "pyroconvective" vertical mixing of O_3 over Alaska and west Canada

[17] The model parameterizations of wet and dry deposition are described by *Giannakopoulos et al.* [1999]. Anthropogenic emissions of NO_x, CO, and NMHCs are based on the values used in the Oxcomp model intercomparison [*Gauss et al.*, 2003]. Lightning emissions use the parameterization of *Price and Rind* [1992] as implemented by *Stockwell et al.* [1999] and are related to the occurrence of model convection, with total emissions of about 5 Tg (N) yr^{-1}. For more details of the emissions see *O'Connor et al.* [2004]. The standard model version uses a monthly mean climatology for the distribution of biomass burning emissions based on the seasonal distribution of *Hao and Liu* [1994] and annual totals from the IPCC Oxcomp [*Gauss et al.*, 2003]. This version of the model was spun up from 1 January 2003 to 1 May 2004.

3.2. Model Outputs

[18] As well as the standard model output of three dimensional fields for the tracers of interest at 30 min intervals, extra outputs were used to investigate the model comparison to aircraft and satellite data, and the ozone budget. Tracer fields were interpolated linearly in space to the aircraft position online in the model (data at 10 s intervals) within each 30-min time step to compare the model simulations to the aircraft measurements. For comparisons to satellite data the 3-D fields of CO and NO_2 are output from the model at the 1030 local time overpass. Tropospheric columns of NO_2 were calculated by the reference sector method (see section 2.2). However, the exact method of subtracting the stratospheric column has little impact on the model agreement with the satellite data [*Savage et al.*, 2004]. Burdens of CO, O_3 and other trace gases within a given region can be calculated from the 3-D tracer fields.

[19] Finally an ozone budget code based on that described by *O'Connor et al.* [2004] was used. Within each time step and grid element of the model the budget code records the change in ozone due to the net chemistry (and the changes due to three major production and three major destruction channels), the change in ozone due to transport (horizontal and vertical advection plus convection and vertical diffusion) and the loss from dry deposition in surface grid elements. Fields of these contributions to the ozone budget due to the different processes are all then output to allow the ozone budget within different regions of the atmosphere to be examined.

3.3. Biomass Burning Emissions

[20] Earlier studies with p-TOMCAT used standard biomass burning emissions with a seasonal variation based on *Hao and Liu* [1994], and contain monthly mean values for an "average" year. This implies that specific events such as the fires which are of interest in this study cannot be accurately represented. To investigate the Alaskan and Canadian wildfires a new emission inventory [*Turquety et al.*, 2007] with daily estimates for North America has been exploited and is used in all the runs described here. The new global inventory is based on more recent investigations, believed to be more accurate, and should provide significantly improved high-latitude biomass burning emissions. Global CO emissions in the new inventory are smaller with only 156 Tg of CO emitted during May to August 2004 (the emissions from south America are much lower), whereas the emission inventory in the same period from our older emission database has 249 Tg of CO.

[21] In the new emission inventory, daily mean emissions of CO, NO_2, formaldehyde, ethane, propane, acetaldehyde and acetone were provided at $1^\circ \times 1^\circ$ resolution for North America. These emissions were calculated using MODIS hot spot data, reported area burned, and information on type of vegetation, fuel loading and emission factors (for more details see *Turquety et al.* [2007]). The biomass burning emissions for the rest of the world during this period were based on the *Yevich and Logan* [2003] inventory, also provided at $1^\circ \times 1^\circ$ resolution, and are monthly mean climatologies not daily data. All the emission inventories were regridded to $2.8^\circ \times 2.8^\circ$ resolution for p-TOMCAT. The old emissions were used to spin the model up but the new inventory was used from 1 May 2004 for all the integrations described in this paper.

3.4. Model Simulations Performed

[22] Four model simulations were performed (see Table 1). The first (run A) excluded the biomass burning emissions from the Alaska and west Canada fires (the region 80.2–170.2°W and 55.8–75.3°N, see rectangular box in Figure 3) to provide a baseline. The other runs all included the fire emissions from the Alaska and west Canada region (CO, NO_2, formaldehyde, ethane, propane, acetaldehyde and acetone). In the inventories the emissions are only from small areas within this region, and the locations of these changed from day to day.

[23] The second simulation (run B) included the emissions from the Alaska and west Canada fires, which were placed uniformly into the troposphere (constant mixing ratio) between the surface and ~250 hPa altitude (the bottom 20 model levels), about 10 km. The fires generated powerful pyroconvection which would have carried the emissions high into the troposphere, and indeed commercial aircraft observed plumes reaching the tropopause (see the photograph in the IGAC Newsletter, issue 32, November 2005). *Damoah et al.* [2006] have also identified pyroconvective events for the Alaska and west Canada fires. Run B is a simple attempt to include the effect of the pyroconvection.

[24] However we expect that the pyroconvection also resulted in substantial lofting of the boundary layer air, containing low O_3, into the fire plumes. So to examine this possibility we carried out a third simulation (run C) in which additional vertical mixing was applied to the O_3

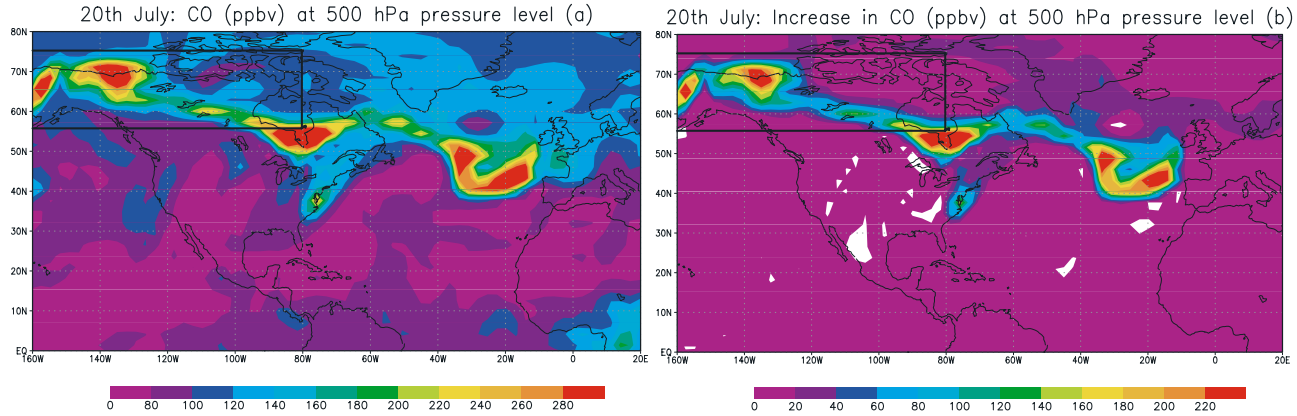

Figure 3. (a) p-TOMCAT tracer field of CO (ppbv) from run D and (b) the increase between runs A and D at 500 hPa on 20 July 2004 (1200 UT). The box represents the region in which the small areas of biomass burning emissions were treated differently between the model simulations.

columns over the fires to produce a uniform profile between the surface and ~250 hPa. This mixing was done every time step, within the Alaska and west Canada region, where the emissions increased surface concentrations of CO by more than 20%. The homogenization of the model profiles over the fires in this simulation is not meant to be an accurate representation of pyroconvection but instead represents a sensitivity study on the impact of the redistribution of tropospheric O_3. In all the simulations the biomass burning emissions in all other regions were confined to the surface and there was no additional vertical mixing of O_3.

[25] The NO_2/CO emission ratio (0.033) in the *Turquety et al.* [2007] inventory is typical of tropical biomass burning [*Duncan et al.*, 2003a] but boreal fires are observed to have a much lower ratio [*Wofsy et al.*, 1992; *Bertschi et al.*, 2004]. *Wofsy et al.* [1992] gave two possible explanations for the low NO_2/CO emission ratio from boreal fires: a greater prevalence of smoldering combustion in the fires and the lower nitrogen concentrations in boreal vegetation. Therefore a fourth model sensitivity calculation (run D) was carried out with NO_2 emissions from the Alaska and west Canada fires reduced by a factor of 4 to investigate the effect on O_3 production. This reduction brings the NO_2/CO emission ratio from the area of the fires down to 0.008, much closer to the estimate for boreal fires by *McKeen et al.* [2002] based on their model simulations of O_3 production combined with measured NO_y. Vertical mixing of O_3 over the fires was also applied, as in run C, and this simulation represents a further sensitivity study of the impact of reducing the NO_2 emitted by the fires.

[26] Next we compare the results from the four simulations to measurements to examine the impact of the long-range transport of the fire emissions on the tracer fields and ozone budgets over north America, the Atlantic and western Europe, and to investigate the sensitivity of the model results to pyroconvective lifting and the specification of the NO_2 emissions.

4. Results

4.1. CO in the Fire Plumes

[27] The ITOP/ICARTT campaign was designed to study the long-range transport of anthropogenic tracers from America, across the Atlantic to Europe and extensive airborne measurements were made in the regions of the east coast of America, the mid-Atlantic and the west coast of Europe (Figure 1). At the same time, the prevailing winds carried the emissions from Alaskan/Canadian fires eastward across Canada, the east coast of the USA and the Atlantic to western Europe. In this section we consider how well the model has simulated the transport of these fire emissions within the fire plumes.

[28] Figure 3 shows the CO tracer field from p-TOMCAT for model run D (3a) and the increases between runs A and D (3b) at 500 hPa on 20 July 2004 (1200 UT), with the region which includes the Alaskan and west Canadian forest fires shown by a rectangle. The CO field shows a line of fire plumes right across Canada and the North Atlantic at 500 hPa originating from the fire emissions, and substantial increases in CO are also seen over the east coast of the USA, Greenland and Iceland, stretching toward Europe.

[29] Figure 4 compares model run D to measurements of CO columns from the MOPITT satellite instrument. The measurements of CO are quite patchy (white areas show no data) as the EOS-Aura satellite only covers about half the globe each day (at 60°N) and pixels with more than 10% cloud cover are rejected. So here the combined measurements from 19, 20 and 21 July 2004 are calculated to maximize the amount of available data and then compared to the mean of the model columns at 1030 local time on the same three days from the simulation. Combining data from more than three days would smooth out the pattern of the fire plumes. The CO field from p-TOMCAT shows the same general pattern of fire plumes over Alaska, Canada and the North Atlantic, and also over Central Africa, as seen by the higher-resolution MOPITT measurements (Figure 4a). For a more detailed comparison p-TOMCAT results from both runs A and D are plotted against the measurements (by averaging the measurements over the coarser model grid) within three regions: The region containing the fire plumes (Alaska and Canada, 49.2–170.2°W and 47.4–75.3°N, and the Atlantic, 9.8–49.2°W and 36.3–61.4°N) (Figure 4b), the USA (63.3–128.0°W and 16.7–47.4°N) (Figure 4c) and Europe (32.3°E–9.8°W and 30.7–64.2°N) (Figure 4d). The results are summarized in Table 2. In all three regions the results from run D are much closer to the MOPITT

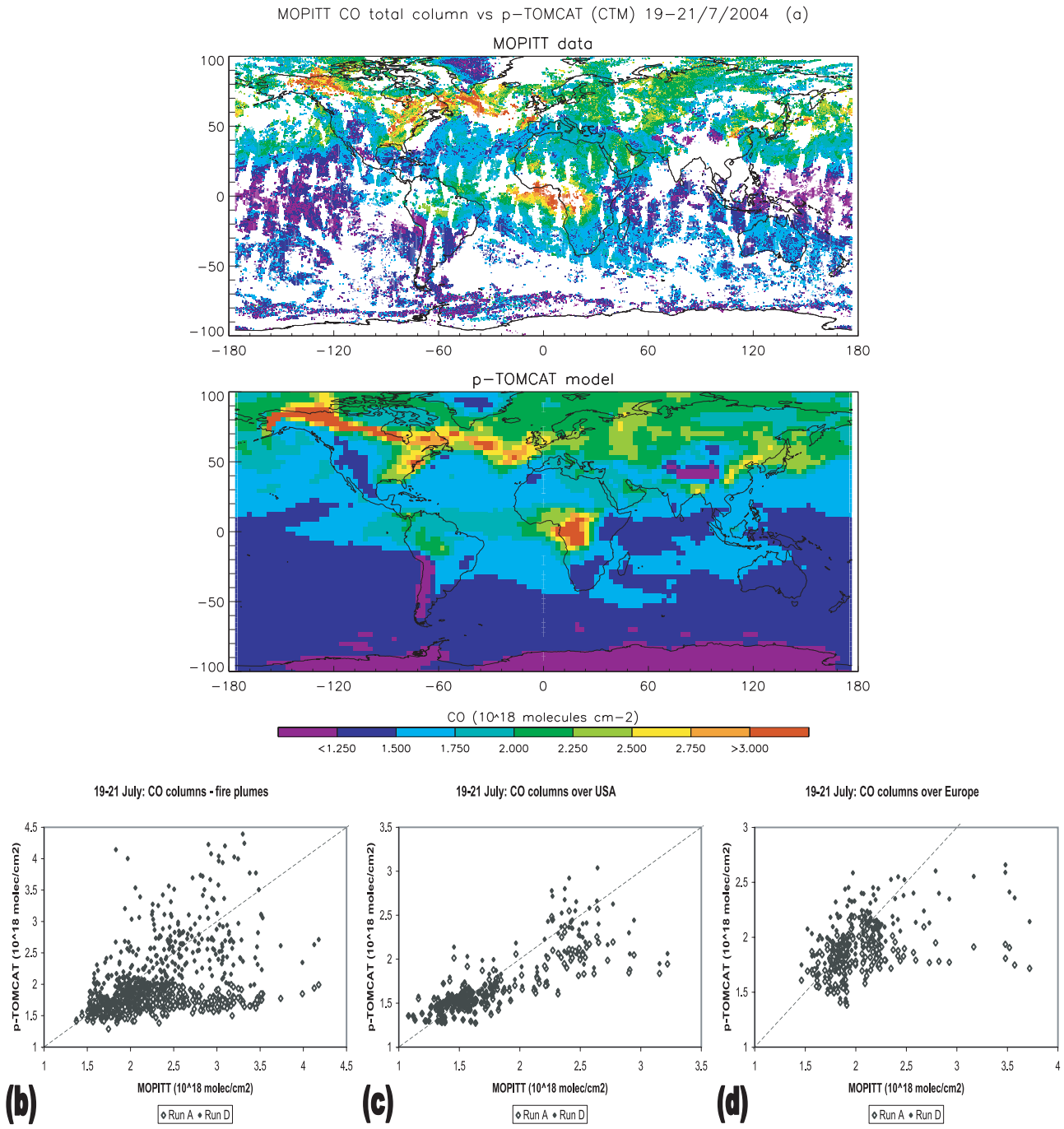

Figure 4. (a) Measurements of CO tropospheric columns from the MOPITT satellite instrument, combined from 19, 20 and 21 July 2004 (white areas show no data), compared to p-TOMCAT results from run D, mean values from the three days. The color bar is the same for both plots (10^{18} molecule cm^{-2}). p-TOMCAT results from runs A and D plotted against the measurements in three regions: (b) fire plumes (9.8–49.2°W, 36.3–61.4°N and 49.2–170.2°W, 47.4–75.3°N), (c) USA (63.3–128.0°W, 16.7–47.4°N) and (d) Europe (32.3°E–9.8°W, 30.7–64.2°N).

measurements than the results from run A, the mean values are improved, the gradients of the orthogonal least squares fits are closer to 1.0, and the R^2 correlation coefficients are increased. So, when a simple treatment of pyroconvective lifting is included (there is little difference in the CO plume between runs B, C and D) the model fire plumes are a good match to the MOPITT measurements in magnitude and location, suggesting not only that the model transport, forced by ECMWF analyses, is accurate but also that the new *Turquety et al.* [2007] CO emissions are reasonable.

[30] Figure 5 shows profiles of the measurements of CO from the three aircraft flights which encountered the intense fire plume. To create this profile mean values in 25 hPa bins were calculated. The plume is clearly observed in the large

Table 2. CO Tropospheric Columns

	Region		
	Fire Plumes	USA	Europe
Mean MOPITT measurement, 10^{18} molecule cm^{-2}	2.27	1.73	2.04
Mean model value, 10^{18} molecule cm^{-2}			
Run A	1.69	1.63	1.81
Run D	2.23	1.70	2.02
Model/measured orthogonal best fit-line gradient			
Run A	0.101	0.542	0.128
Run D	1.224	0.824	0.542
R^2 correlation coefficient			
Run A	0.176	0.670	0.064
Run D	0.405	0.701	0.360

CO values in a narrow filament around 400 hPa measured by the DC8 on 18 July (Figure 5a) and in a much thicker layer between 600 and 400 hPa measured by the BAe-146 on 20 July (Figure 5b). Data from the DLR Falcon flying close to Europe on 23 July shows a plume between 550 and 475 hPa with evidence for enhanced CO values down to 825 hPa (Figure 5c), possibly indicative of mixing downward from the main plume. Figure 5 also shows the mean values from the four model simulations. Run A, without the boreal fire emissions, has much lower CO than measured and completely fails to model the plume. Model CO values from the integrations with the fire emissions are much larger, particularly at the plume altitudes, and match the measurements from the DC8 (Figure 5a) and the BAe-146 (Figure 5b) quite closely (there is little difference between runs B, C and D here). In particular, simulation of the DC8 measurements reproduces the thin plume around 400 hPa while the plume over the mid-Atlantic, where it was intercepted by the BAe-146, is much deeper. However, over Europe the model profiles have little structure in contrast to the observations (Figure 5c). Detailed investigation of the model 3-D tracer fields shows strong convective mixing of the fire plume when it reaches the west coast of Europe on 22 July (and see in section 4.2 the discussion of the NO profile at this location). Convection may be too vigorous because of the low spatial resolution of the model causing spurious convection over what are in reality maritime areas. Although the high CO concentrations in the measured profile around 750 hPa are perhaps evidence of vertical mixing, it is clear that the model is overestimating this effect.

[31] Despite the poor agreement with the DLR Falcon data, which as discussed appears to arise in the model from too vigorous convection over Europe, comparison between the model and measurements from MOPITT and the DC8 and BAe-146 aircraft suggest that the large-scale horizontal extent of the plume is captured well in the model from its origin over Alaska and Canada until it reaches continental Europe. We conclude that the model large-scale transport, driven by the ECMWF analyses is accurate and the new CO emissions inventories are realistic in both size and location.

4.2. Chemistry in the Fire Plumes

[32] In this section we consider the chemistry within the fire plumes by comparing the model values of NO_2, NO, O_3, PAN, NO_y and peroxy radicals with available measurements.

[33] Figure 6 shows the model O_3 and NO_x fields from run D and the increase between runs A and D at 500 hPa on 20 July (1200 UT). The region containing the Alaskan and west Canadian fires is shown by the rectangle. A major feature in Figure 6a is an ozone plume stretching from northern Canada over Greenland into the Atlantic. This feature is also found in run A. It has no connection with the boreal fires and it was not sampled by the aircraft.

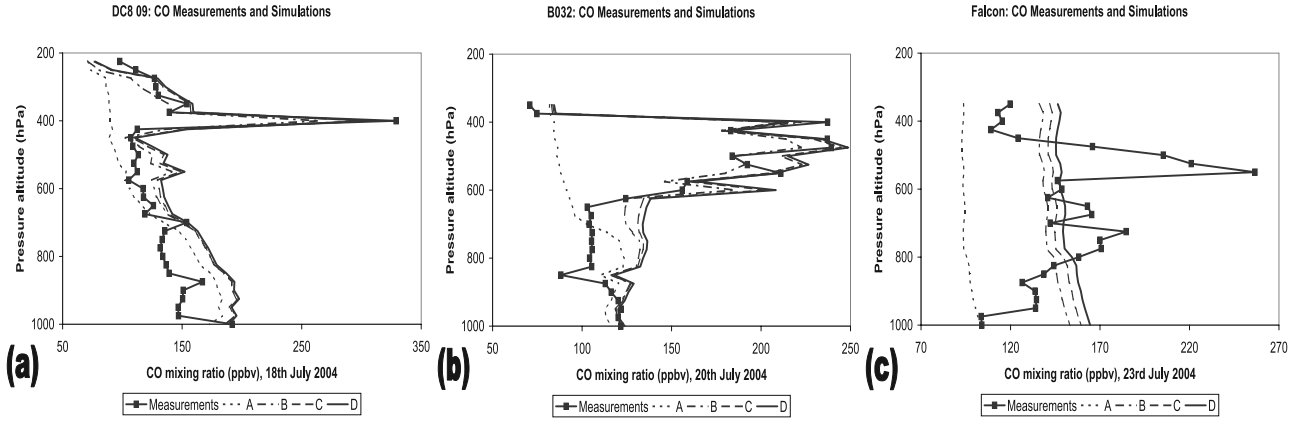

Figure 5. Measurements of CO (ppbv) versus pressure altitude (hPa) from (a) DC8 flight 09 on 18 July 2004, (b) BAe-146 flight B032 on 20 July and (c) the DLR Falcon flight on 23 July (lines with data points), along the flight tracks shown in Figure 1. With p-TOMCAT results from the four simulations, run A (dotted lines), run B (dashed lines), run C (dot/dash lines) and run D (continuous lines).

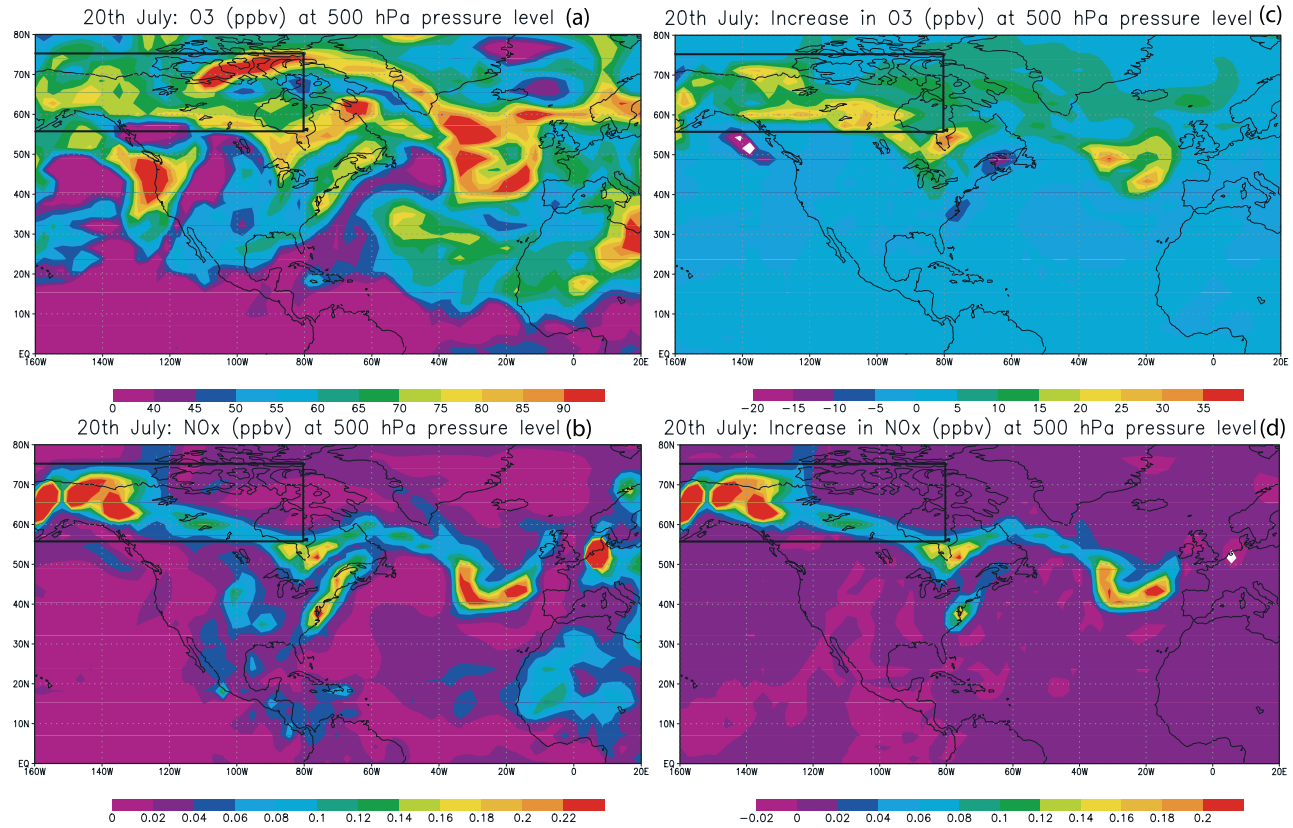

Figure 6. p-TOMCAT tracer fields of (a) O_3 and (b) NO_x (ppbv) from run D, and the increases in (c) O_3 and (d) NO_x between runs A and D, at 500 hPa on 20 July 2004 (1200 UT). The box represents the region in which the small areas of biomass burning emissions were treated differently between the model simulations.

A second, more southerly filament seen in Figure 6a is associated with the fires and this is the focus of our study. The plume is seen more clearly in Figures 6c and 6d which show increases in O_3 and NO_x between runs A and D. The increases across Alaska, Canada and the North Atlantic coincide with the CO plume in Figure 3, and there is also enhanced NO_x over the east coast of the USA. Further south there are regions of reduced O_3 resulting from the additional vertical mixing of O_3 in run D.

[34] Figure 7 compares the measurements of NO_2 tropospheric columns from the SCIAMACHY satellite instrument to model columns from run D. As with MOPITT on EOS-Aura, the coverage of NO_2 from the ENVISAT satellite is incomplete (white areas showing no data), and in addition SCIAMACHY alternates between nadir (for columns) and limb sounding while MOPITT is nadir only. So, again, the measurements and model columns from 3 days are each combined in Figure 7 to maximize the available data while retaining the signal of the fire plumes. Estimates of the NO_2 in the stratosphere have been subtracted at each model latitude band to match the processing of the measurements.

[35] Both the measurements and model results show enhanced NO_2 across Canada and the North Atlantic, but the fire plumes are much less pronounced than for CO (Figure 7a). Also the model values over land are too large. This is consistent with the study of *Savage et al.* [2004] in which NO_2 columns from the GOME instrument were compared to TOMCAT results finding a good overall correlation, but with model columns too large over polluted areas. This is probably a consequence of the lack of higher VOCs in the model which would otherwise help to remove NO_2 either directly by forming PAN or indirectly by reacting with O_3 to form radicals.

[36] We focus on the same three regions as in Figure 4 (the fire plumes (Figure 7b), the USA (Figure 7c) and Europe (Figure 7d)) for a more detailed comparison, plotting the values from runs A and D against the SCIAMACHY measurements (by averaging the measurements over the coarser model grid). The results are set out in Table 3. In the fire plumes region the mean value from run D is much closer to the measurements than the mean value from run A. There is more scatter in the model values than for the CO in the plumes (Figure 4b), there is little change in the gradient of the orthogonal least squares fit and the R^2 correlation coefficient is reduced. In the regions of the USA and Europe the mean model values and gradients are much too high because of the high model values over polluted areas, and there is little change between model runs A and D because NO_2 from the fire emissions is much less than from the anthropogenic emissions.

[37] Figure 8 shows the vertical profile of NO, O_3, PAN and NO_y measured on the three flights which encountered the large fire plume, again with mean values calculated in 25 hPa bins and compared to the four model simulations. The DC8 measurements of NO_y here are the sum of the NO,

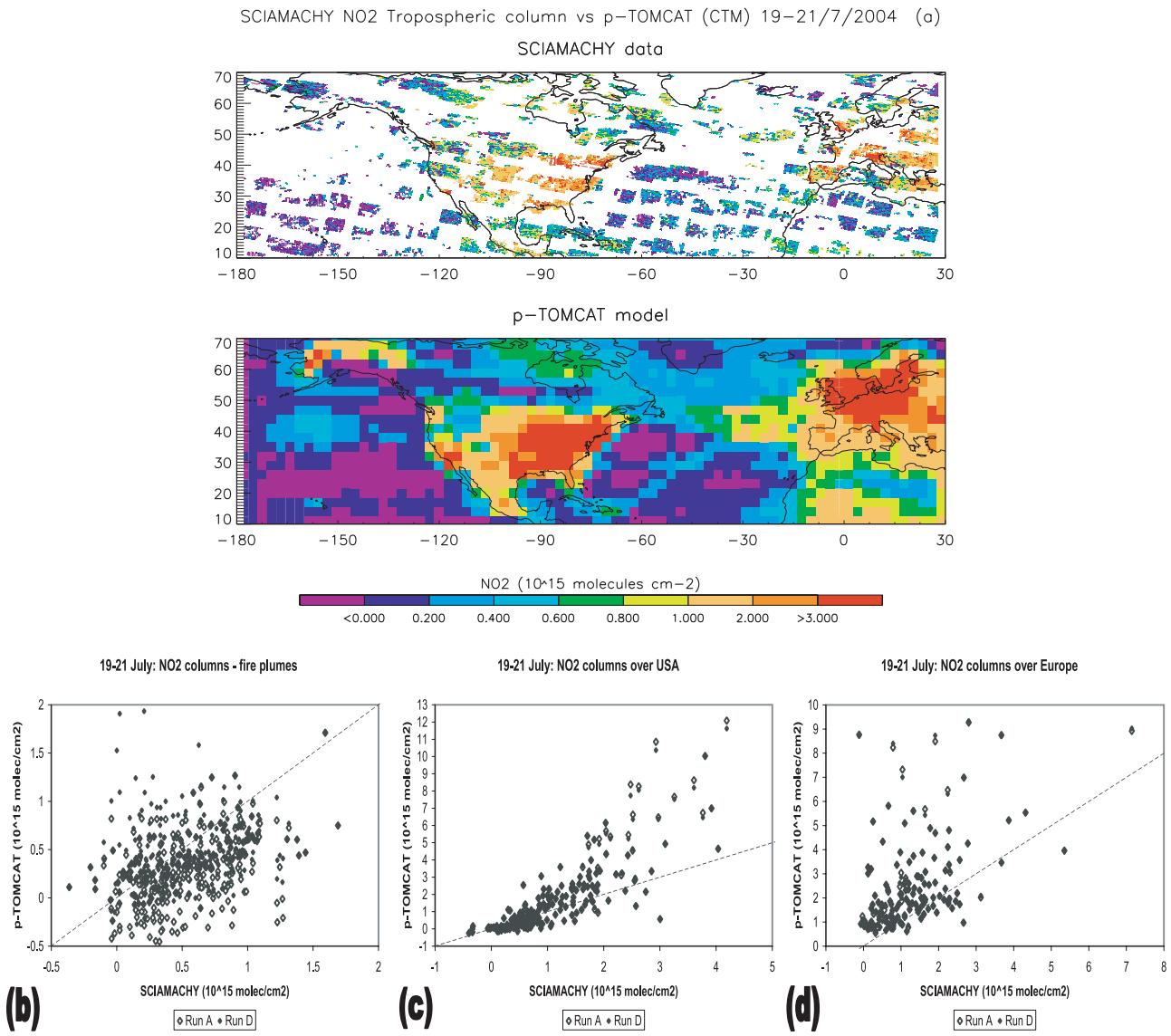

Figure 7. (a) Measurements of NO_2 tropospheric columns from the SCIAMACHY satellite instrument, combined from 19, 20 and 21 July 2004 (white areas showing no data), compared to p-TOMCAT results from run D, mean values from the three days. Same color bar for both plots (10^{15} molecule cm^{-2}). p-TOMCAT results from runs A and D plotted against the measurements in three regions: (b) fire plumes (9.8–49.2°W, 36.3–61.4°N and 49.2–170.2°W, 47.4–75.3°N), (c) USA (63.3–128.0°W, 16.7–47.4°N) and (d) Europe (32.3°E–9.8°W, 30.7–64.2°N).

NO_2, PAN and HNO_3 measurements from this flight. There were no NO_y measurements from the BAe-146 flight and no PAN measurements from the DLR Falcon flight.

[38] The structure of the plume as seen in CO (Figure 5) is confirmed by the measurements shown in Figure 8. At the location close to the east coast of the USA sampled by the DC8, the plume is narrow but clearly evident in the elevated measurements of PAN (Figure 8g) and NO_y (Figure 8j). At the same pressure, the DC8 measured a thin layer with slightly reduced ozone. Evidence for a plume in NO is not strong. Over the mid-Atlantic, the plume has a much greater vertical extent. Ozone (Figure 8e) and PAN (Figure 8h) concentrations are elevated. There was no NO_y measurement at this location and the NO measurements cannot be interpreted unambiguously as showing evidence of a plume. The DLR Falcon measurements close to Europe are consistent with the CO measurements there; there is evidence of a plume at about 550 hPa in ozone (Figure 8f) and NOy (Figure 8l) as well as high concentrations at higher pressures, perhaps related to downward mixing out of the plume. For the DC8 and BAe-146 measurements, the model results shown in Figure 8 reproduce the structure of the observed plume; we discuss the magnitudes below. The plume close to Europe is poorly modeled. Notice that all the modeled NO profiles close to Europe (Figure 8c) show a classical C-shape, typical of the effect of convection. The poor model performance is clearly related to an overestimate of convective activity at this location.

[39] The chemistry in the plume will, of course, be affected by the extent of the emissions (CO, VOCs, NO_2)

Table 3. NO_2 Tropospheric Columns

	Region		
	Fire Plumes	USA	Europe
Mean SCIAMACHY measurement, 10^{15} molecule cm^{-2}	0.52	1.11	1.23
Mean model value, 10^{15} molecule cm^{-2}			
Run A	0.28	1.68	2.39
Run D	0.45	1.67	2.41
Model/measured orthogonal best fit-line gradient			
Run A	0.935	2.67	2.86
Run D	0.876	2.58	2.82
R^2 correlation coefficient			
Run A	0.187	0.702	0.249
Run D	0.076	0.712	0.253

into the plume. Our set of integrations was designed to look in particular at how much of the emissions were lifted into the middle free troposphere and how much NO_2 was emitted. We have already argued in section 4.1 that the model CO emissions from the fires are realistic.

[40] Figure 8j shows the modeled NO_y at the DC8 location. Simulation A does not show a plume but simulations B, C and D do. However, the observed NO_y is significantly overestimated in runs B and C. In contrast, experiment D, with reduced NO_2 emissions in the boreal fires, corresponds much better to the observations. Thus the DC8 measurements support the idea [*McKeen et al.*, 2002] that boreal fires have a lower NO_2/CO emission ratio than fires at lower latitudes. Unfortunately there is no NO_y data from the BAe146 and the comparison with the DLR Falcon data is affected by the model convection. However, peak NO_y in the DLR plume is 2 ppbv, in a narrow layer. If we assume that NO_y is conserved in the plume, then the maximum NO_y observed at the location of the BAe-146 should not have been greater than 2 ppbv. It seems clear that runs B and C (Figure 8k) give an overestimate of NO_y, again supporting the lower NO_2 emissions.

[41] In general the DC8 ozone profile is reproduced well by all the model runs (Figure 8d) but the larger concentrations in runs B and C at the altitude of the plume are not observed. Indeed, for the DC8 flight the measurements of O_3 show no enhancement at altitudes around 400 hPa; in fact, O_3 was slightly reduced. This suggests that there were very low ozone production rates or even slight ozone destruction in this part of the plume. Model runs A and D give much better comparison to the observations although none of the model runs captures the small decrease at the altitude of the plume. For the BAe-146 flight (Figure 8e) there is a large overestimate of the ozone concentrations in the plume for runs B and C (though run C, with additional vertical mixing of ozone from the boundary layer, reduces the peak in model O_3) and much better agreement for runs A and D. This is consistent with the results of *Wofsy et al.* [1992] and *Bertschi et al.* [2004] who also measured low $\Delta O_3/\Delta CO$ ratios in boreal fire plumes.

[42] Our sensitivity studies show that the model can simulate the low $\Delta O_3/\Delta CO$ ratio in the observed plume, but suggests that both the vertical mixing of O_3 by pyroconvection and the lower NO_2/CO emission ratio are needed. The comparison of model O_3 profiles with measurements from the DLR Falcon flight (Figure 8f) is poor for reasons which have already been discussed. However, we note that model runs B and C overestimate the ozone here.

[43] Our argument for reduced NO_2 emissions is based in part on the NO_y measurements from the DC8, which are clearly overestimated in the model when the higher NO_2 emissions are employed (and is supported by inferences based on the DLR Falcon data). However, the chemistry in the plume is also affected by how NO_y is partitioned between NO_x and reservoir species. From the DC8 measurements more than half of the NO_y in the plume was in the form of PAN (Figures 8g and 8j), and the similar concentrations of PAN (Figure 8h) and NO_y (Figure 8l) measured in the plume over the mid-Atlantic and Europe imply that there has been little removal of NO_y over 1000s of km and several days. (*Wofsy et al.* [1992] found a high conversion of NO_x to reservoir species in sub-Arctic fire plumes due to high concentrations of reactive hydrocarbons). The model chemistry scheme has only a limited VOC mechanism and does not, for example, include isoprene, so that in general the production of PAN in the model is too low. For example, within the model chemical mechanism acetaldehyde (CH_3CHO) can be oxidized to form PAN, and while the biomass burning emissions contain acetaldehyde (5 Tg yr^{-1} in the inventories) this leads to too little PAN in the model simulations (Figures 8g and 8h) and more acetaldehyde is needed from the oxidation of VOCs. The lack of VOCs and the associated reduction in PAN formation is, at least in part, a possible alternative explanation for the concentrations of NO_x and O_3 within the model plume being too high.

[44] Unlike for CO, no clear plume is seen in the NO observed by any of the three flights. In contrast, for model runs B and C the modeled concentrations of NO for the DC8 and BAe-146 (Figures 8a and 8b) show enhanced concentrations at the same altitude as the peak concentrations of CO. This high NO_x could then explain the high ozone modeled over the mid-Atlantic (Figure 8e). However, the NO concentrations in runs A and D match the observed profiles of NO much better. Either the NO_2 emissions in the *Turquety et al.* [2007] inventory are too great and a lower NO_2/CO emission ratio closer to the value of 0.007 estimated by *McKeen et al.* [2002] matches these fires more closely, or much more of the emitted NO_2 was converted to PAN. For the DLR Falcon flight over western Europe the four model runs give very similar results for NO indicating that here, after a few days, the modeled impact of the fires on the NO profile is small and conversion to model reservoir species, mainly HNO_3 but also PAN, is complete. In addition all the model runs have higher NO concentrations than the observations. Detailed investigation of the model 3-D tracer fields for 23 July shows large vertical

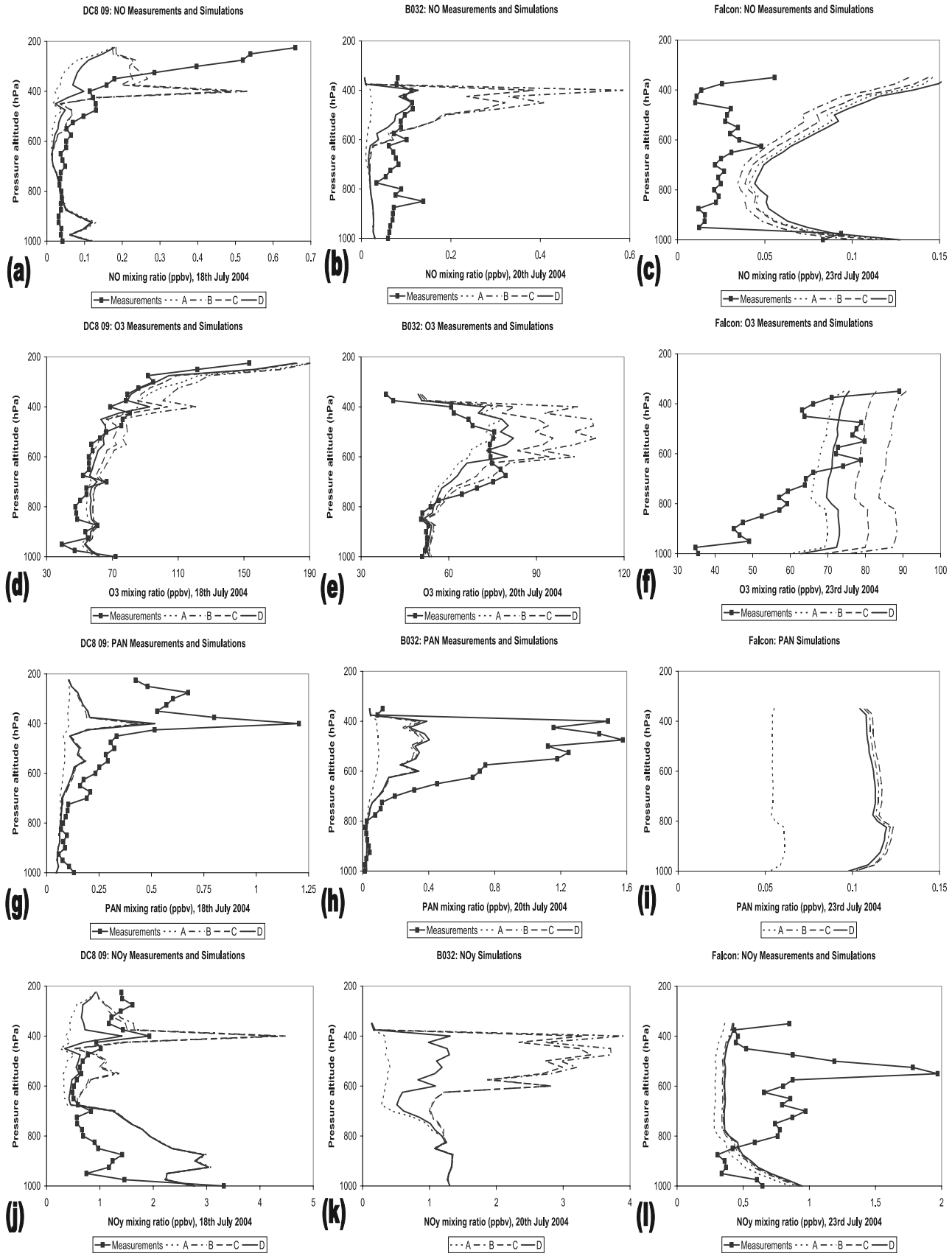
DC8 09: NO Measurements and Simulations
B032: NO Measurements and Simulations
Falcon: NO Measurements and Simulations
Pressure altitude (hPa)
(a)
NO mixing ratio (ppbv), 18th July 2004
(b)
NO mixing ratio (ppbv), 20th July 2004
(c)
NO mixing ratio (ppbv), 23rd July 2004
Measurements A B C D
DC8 09: O3 Measurements and Simulations
B032: O3 Measurements and Simulations
Falcon: O3 Measurements and Simulations
(d)
O3 mixing ratio (ppbv), 18th July 2004
(e)
O3 mixing ratio (ppbv), 20th July 2004
(f)
O3 mixing ratio (ppbv), 23rd July 2004
DC8 09: PAN Measurements and Simulations
B032: PAN Measurements and Simulations
Falcon: PAN Simulations
(g)
PAN mixing ratio (ppbv), 18th July 2004
(h)
PAN mixing ratio (ppbv), 20th July 2004
(i)
PAN mixing ratio (ppbv), 23rd July 2004
DC8 09: NOy Measurements and Simulations
B032: NOy Simulations
Falcon: NOy Measurements and Simulations
(j)
NOy mixing ratio (ppbv), 18th July 2004
(k)
NOy mixing ratio (ppbv), 20th July 2004
(l)
NOy mixing ratio (ppbv), 23rd July 2004

Figure 8

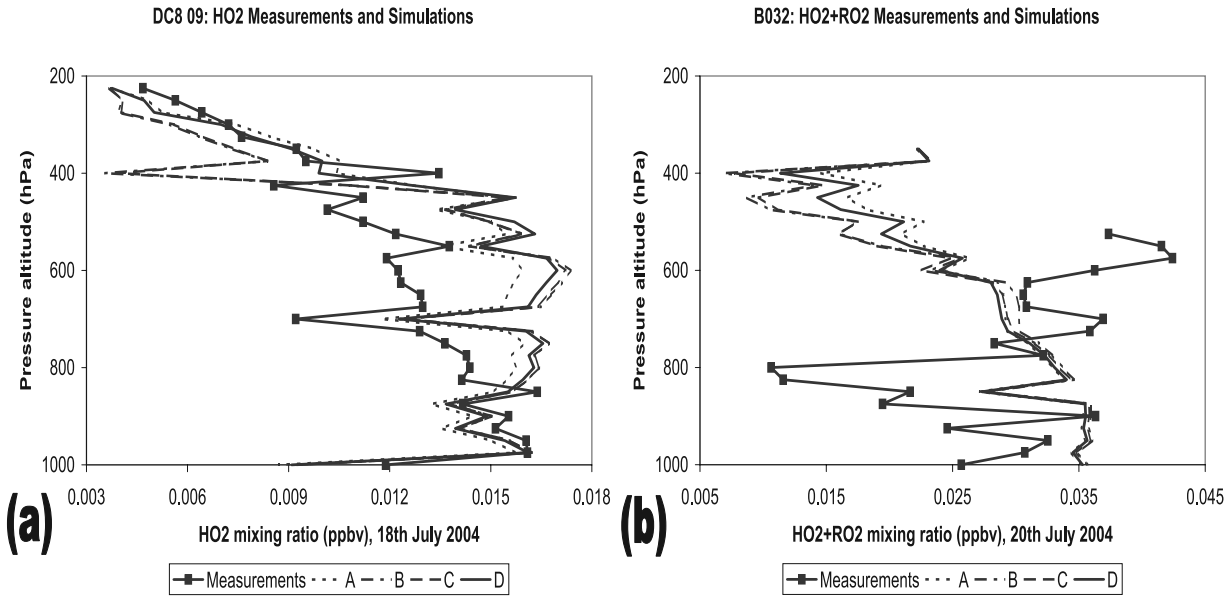

Figure 9. Peroxy radicals (ppbv) plotted against pressure altitude (hPa) (a) from DC8 flight 09 on 18 July 2004 (HO_2) and (b) from BAe-146 flight B032 on the 20 July (HO_2 + RO_2) (lines with data points), along the flight tracks shown in Figure 1. With p-TOMCAT results from the four simulations, run A (dotted lines), run B (dashed lines), run C (dot/dash lines) and run D (continuous lines). There were no peroxy radical measurements from the DLR Falcon.

mixing over Europe bringing up NO_x from the surface and also bringing down NO_x from the stratosphere.

[45] Furthermore, as we have already discussed, NO_y in the model plume is too high in runs B and C compared to the DC8 measurements, while NO_y in run D is much closer to the observations but is somewhat on the low side. If too little PAN formation was the reason for the excess model NO_x in the plume (e.g., in runs B and C) we would expect that the modeled NO_y would be about the same or lower than that observed (since the lifetime of NO_x is shorter than that of PAN). The higher than observed modeled NOy for the DC8 flight thus gives support to the hypothesis that it is the emissions of NO_2 in runs B and C which are too high. It is also clear that the formation of PAN in our model plumes is relatively insensitive to the emissions of NO_2 (PAN concentrations are very similar in runs B, C and D) which suggests that the formation of PAN is limited by the formation of peroxyacetyl radicals. Although PAN formation is a key outstanding issue in the model chemistry, it cannot alone explain the high NO_x concentrations in the model plume.

[46] To examine further the chemistry within the fire plume the measurements of HO_2 from the DC8 flight and total peroxy radicals (HO_2 + RO_2) from the BAe-146 flight are plotted in Figure 9 along with the results from all four model simulations. The fire plume contained high concentrations of peroxy radicals, observed by the DC8 around 400 hPa (Figure 9a) and by the BAe-146 above 625 hPa (Figure 9b). However, all the model simulations have much lower peroxy radicals within the plume, and runs B and C show a strong decrease. This is partly due to the too high NO_x within the model plumes that would remove radicals, although this can only be part of the explanation for the large deficit, and the high concentrations of PAN observed at these altitudes suggests there should be much higher concentrations of VOCs which would form both PAN and peroxy radicals. Outside of the plume the general shape of the HO_2 profile from the DC8 measurements is reproduced by the model runs, and a rapid decrease in the concentrations at about 700 hPa is seen in both the observations and the model. All the simulations have large peroxy radical values between 700 and 450 hPa compared to the DC8 measurements, and also too high peroxy radical values below 775 hPa compared to the BAe-146 measurements, and this is probably due to the too low NO_x values in the model simulations at these altitudes.

[47] We have shown that model O_3 is sensitive to additional vertical mixing of O_3 (run C) and to the amount of NO_x (run D), with more NO_x producing more O_3 (although the relationship is not linear since the chemical production of O_3 is more efficient at low NO_x concentrations). In model run D the O_3 and NO values within the fire plume are closest to the aircraft measurements, but model PAN is much too low because of a lack of VOCs. Additional PAN

Figure 8. Measurements of (a–c) NO, (d–f) O_3, (g–i) PAN and (j–l) NO_y (ppbv) versus pressure (hPa) from DC8 flight 09 on 18 July 2004, BAe-146 flight B032 on 20 July and the DLR Falcon flight on 23 July (lines with data points), along the flight tracks shown in Figure 1. With p-TOMCAT results from the four simulations, run A (dotted lines), run B (dashed lines), run C (dot/dash lines) and run D (continuous lines). There were no NOy measurements from the BAe-146 and no PAN measurements from the DLR Falcon.

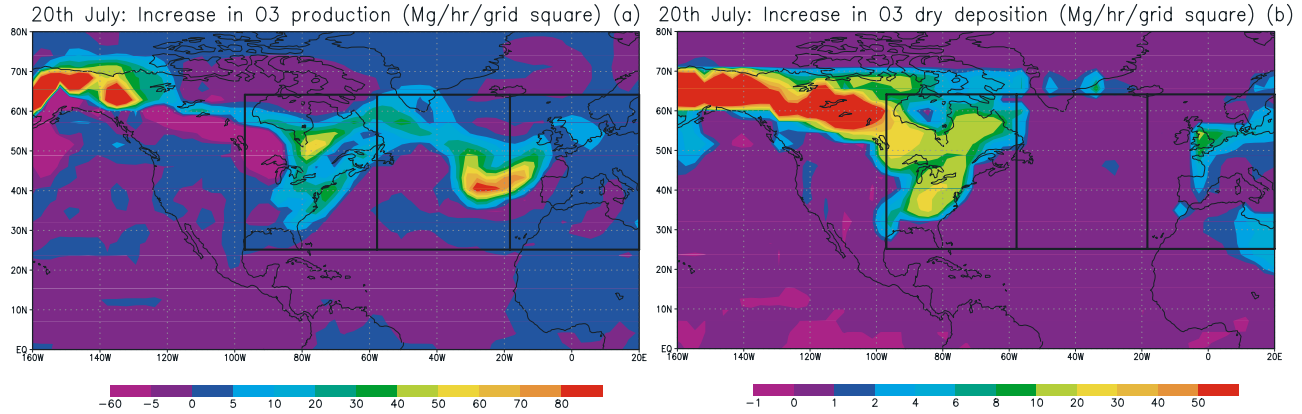

Figure 10. Increase (a) in O_3 net chemical production (from the surface to ~250 hPa) and (b) in O_3 dry deposition at the surface (Mg/hr/2.8° × 2.8° grid square), difference between model runs A and D during 20 July 2004. The rectangles show the eastern USA, mid-Atlantic and western Europe regions.

would be expected to produce more O_3 further downwind as it decomposes in lower altitudes to release NO_x [see *Hudman et al.*, 2004], and *Real et al.* [2007] attribute the enhanced O_3 observed by the DLR Falcon to PAN decomposition during the descent of the fire plume toward Europe. In these sensitivity studies run D best simulates the increased O_3 resulting from the Alaskan and west Canadian fire emissions, although this has to be considered as a lower limit because of the lack of PAN. Model runs B and C, with much higher NO_2 emissions, have O_3, NO and NO_y values in the model plume much larger than the aircraft measurements, and so have to be considered as upper limits to the increased O_3 resulting from the fire emissions. Note that a further source of error in the model simulations could be the low resolution of the model acting to smooth out the NO_x fields which, given the nonlinear relationship between NO_x concentration and O_3 production, could result in an overestimate of the O_3 concentrations.

4.3. Modeled Impact of Fire Emissions on Northern Hemisphere Tropospheric Ozone

[48] In this section we compare the four model simulations to examine the increase in the tropospheric burden of CO and NO_x due to the Alaska and west Canada fires over selected regions of the Northern Hemisphere, and the resulting increase in the model O_3 burden. By examining the differences between run A and the three other runs we can study the sensitivity of the O_3 budget to additional vertical mixing of O_3 and to the amount of NO_2 emitted. Figure 10 shows the difference between simulations A and D in the model net chemical production of O_3 in the bottom 20 model levels (from the surface to ~250 hPa), and in the dry deposition at the surface, during 20 July 2004. Increased O_3 production is seen over Alaska, Canada and the North Atlantic, which matches the patterns of increased CO and NO_x in Figures 3 and 6. Increased dry deposition occurs in Alaska, Canada, the Eastern USA, Western Europe and North Africa. There are also large regions of increased O_3 destruction over parts of Alaska and Canada, due to the additional vertical mixing increasing O_3 near to the surface, which is also responsible for most of the increased dry deposition in Alaska and Canada.

[49] The increased production, loss and burden of O_3 within the model Northern Hemisphere from the surface to ~250 hPa resulting from the fire emissions is now examined in detail. Figures 11a–11c show the increased burdens of CO (Tg), NO_x (Gg N) and O_3 (Tg) in the whole of the model Northern Hemisphere troposphere resulting from the fire emissions; Figures 11d–11f show the increased production and loss of O_3 (Tg). The values are the differences between model runs B, C and D and run A during 50 days from 15 June to 3 August 2004. NO_x in the model has a strong signal for each of the different episodes of fire emissions in the new inventories (Figure 2) while the longer-lived CO and O_3 rise and then fall more slowly in the model runs.

[50] The largest increase in O_3 is in model run B. The increase is not so great in runs C and D where additional vertical mixing changes the O_3 profile. The mixing reduces the O_3 concentrations at higher altitudes up to ~250 hPa by the lofting of near-surface air with low O_3, which shifts the chemical balance here in favor of increased net chemical production, and increases the O_3 concentration near the surface, which shifts the balance to reduced net production, increases dry deposition, and also increases OH radicals leading to a faster removal of CO and NO_x. While the increase in the net chemical production of O_3 over the 50 days is greatest overall in run C (Table 4), dry deposition is also greater and the maximum increase in O_3 is reduced by almost a third between runs B and C because of the additional vertical mixing.

[51] Run D with low NO_2 emissions has a smaller increase in net O_3 production over the 50 days and in this less oxidizing environment more CO remains. Dry deposition is again large because of vertical mixing giving higher O_3 concentrations at the surface. The peak in increased O_3 is reduced by two thirds from run C by the lower NO_2 emissions and occurs later (31 July). Note that O_3 production seems to be more efficient in run D where although NO_2 emissions have been reduced by a factor of 4 the resulting increase in O_3 is only reduced by a factor of 3. In section 4.2 runs B and C are considered to give upper limits for the total O_3 produced by the fire emissions while run D is considered to give a lower limit, so the peak increase in

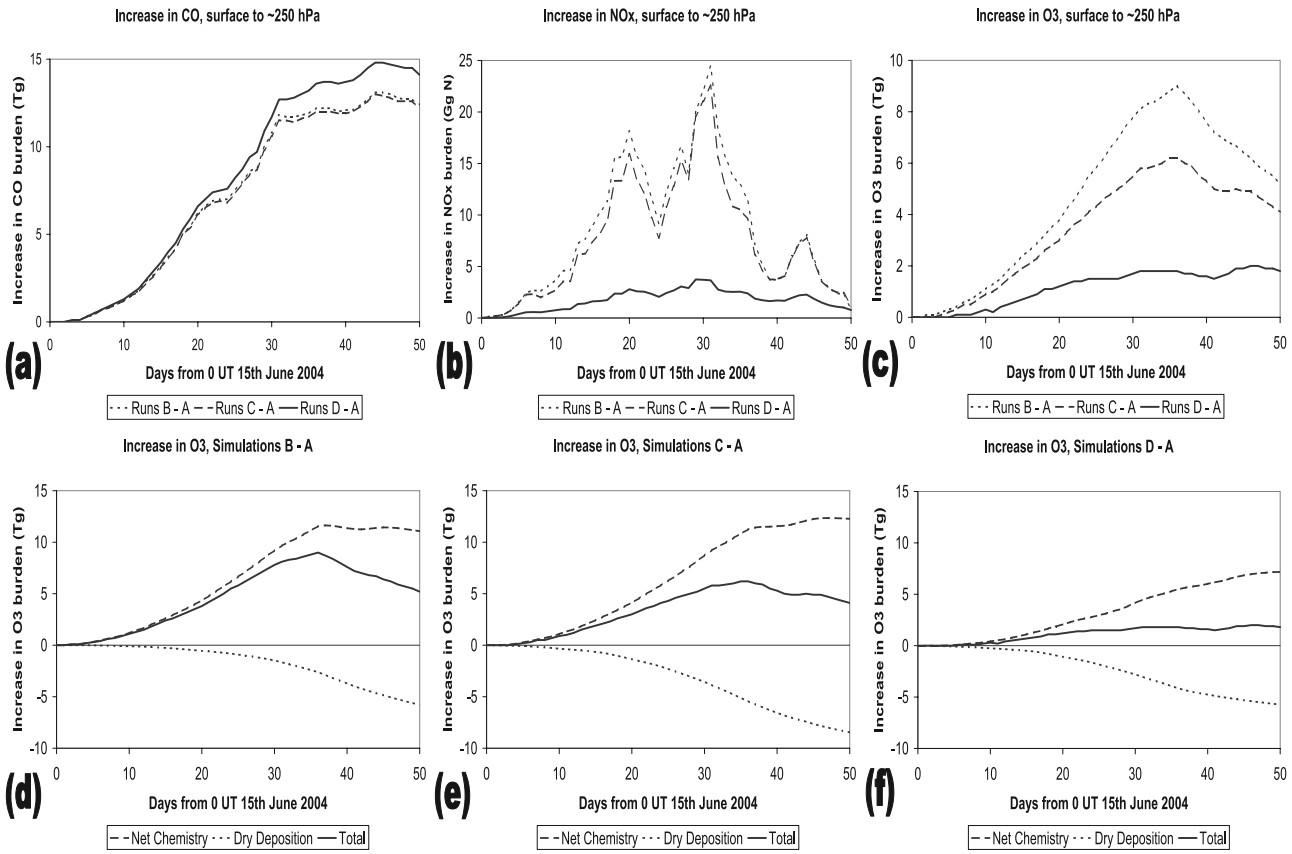

Figure 11. Increase in burdens of (a) CO (Tg), (b) NO_x (Gg N) and (c) O_3 (Tg) within the model Northern Hemisphere (from the surface to ~250 hPa), plotted as differences between model runs A and B (dotted lines), C–A (dashed lines) and D–A (continuous lines) over 50 days from 15 June 2004 (0000 UT). Increase in (d) O_3 (Tg) burdens between runs B–A, (e) C–A and (f) D–A from net chemistry alone (dashed lines), loss from dry deposition alone (dotted lines) and total change (continuous lines) over the 50 days.

the O_3 burden over the Northern Hemisphere is in the range 2.0 (for run D) to 6.2 Tg (for run C), over the Northern Hemisphere burden of about 150 Tg (O_3) in run A. These increases in ozone burden are significant when compared to a projected increase in annual global tropospheric ozone burden from 2000 to 2030 of 20 Tg (O_3) (this is for a scenario assuming the current legislation on emissions of ozone precursors is implemented [*Stevenson et al.*, 2006]). Furthermore the boreal fires over a period of 3 months caused an increase in the ozone burden comparable to the increase of 6–8 Tg (O_3) in the tropics during the Indonesian wildfires, found by *Chandra et al.* [2002] and the 9 Tg (O_3) annual mean from African biomass burning, found by *Aghedo et al.* [2006].

[52] We now consider three regions of equal area, the eastern USA, the mid-Atlantic and western Europe. Figures 12a and 12b show the increase in CO and O_3 burdens (Tg) between model runs A and D within these three regions between the surface and ~250 hPa during the 50 days. With the prevailing west to east wind there is a time delay of about 2 days between the regions, so on the plots the values from the mid-Atlantic have been advanced by 2 days and the values for western Europe by 4 days to help with the comparisons. Figures 12c and 12d show the increased production and loss of O_3 (Tg) between runs A and D within the eastern USA and western Europe regions due to net chemistry, transport from/to other regions, and dry deposition.

Table 4. Increase in Northern Hemisphere Tropospheric Ozone[a]

	Simulations B–A	Simulations C–A	Simulations D–A
Increase in net chemical production over 50 days	+11.1	+12.3	+7.2
Increase in net transport over 50 days	−0.2	+0.2	+0.3
Increase in dry deposition over 50 days	−5.8	−8.5	−5.7
Increase in tropospheric burden over 50 days	+5.2	+4.1	+1.8
Peak increase in tropospheric burden (percent peak increase over run A)	+9.0, 6.0%	+6.2, 4.1%	+2.0, 1.3%

[a]Unit is Tg.

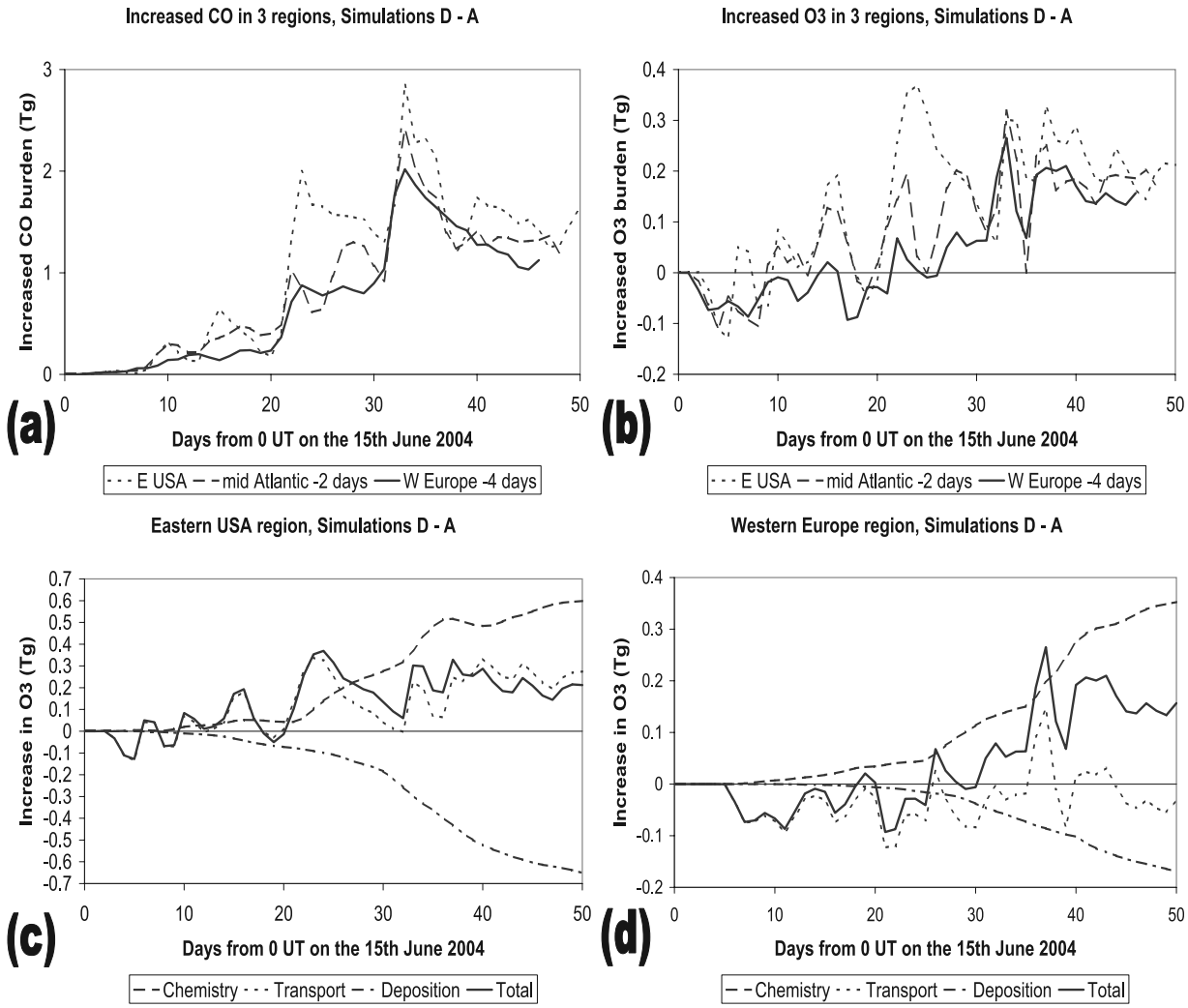

Figure 12. Increase in model burdens of (a) CO and (b) O_3 (Tg) between runs A and D within the eastern USA (dotted lines), mid-Atlantic (dashed lines) and western Europe (continuous lines) regions, from the surface to ~250 hPa, during the 50 days from 15 June 2004 (0000 UT). The mid-Atlantic lines are advanced by 2 days and western Europe lines by 4 days to remove the 2 day time lag between the regions. Increase in model O_3 (Tg) burdens within the (c) eastern USA and (d) western Europe regions between runs A and D from net chemistry alone (dashed lines), transport from/to other regions alone (dotted lines), loss from dry deposition alone (dot/dash lines) and total change (continuous lines) during the 50 days.

[53] The increases in CO and O_3 rise and fall within each region as the plumes from different episodes of the fire emissions enter and leave. Some of the air masses have reduced O_3 compared to the baseline run A, due to the additional vertical mixing redistributing O_3 and leading to increased dry deposition, and this is particularly seen at the start of the period. Over the first 20 days in the eastern USA region (24 days in the western Europe region) the increases in the CO and O_3 burdens and in net chemical production and dry deposition of O_3 are small, but after this time they become much greater with further increases from large episodes of pollution. While the emissions increase over the first 20 days (Figure 2) the greater increases after this time may also be from the meteorology bringing more of the emissions to the three regions. The increased burdens of CO and O_3 peak around 18 July over the eastern USA, on 20 July over the mid-Atlantic and on 22 July over western Europe which coincides with the track of the intense fire plume.

[54] The additional burdens of CO and O_3 from the fires decline from west to east (highest in the eastern USA and lowest in western Europe) because of a combination of photochemistry and mixing. The increase in net chemical production and dry deposition of O_3 also declines from west to east. However, the increased net chemical production of O_3 remains quite large over western Europe and still gives a large increase in the O_3 burden even with both transport and dry deposition removing O_3. The increase in the O_3 burden is very similar within the three regions (Table 5) even though the distances from the fires are very different. The results from model run D are perhaps low estimates for the amount of O_3 produced from the fire emissions (since run D

Table 5. Increase in Tropospheric Ozone Within Three Regions[a]

	Eastern USA	Mid-Atlantic	Western Europe
Increase in net chemical production over 50 days	+0.60	+0.35	+0.35
Increase in net transport over 50 days	+0.27	−0.10	−0.03
Increase in dry deposition over 50 days	−0.65	−0.05	−0.17
Increase in tropospheric burden over 50 days	+0.21	+0.17	+0.16
Peak increase in tropospheric burden (percent peak increase from run A to run D)	+0.37, 3.8%	+0.32, 3.3%	+0.27, 2.6%

[a]Unit is Tg.

has too little PAN compared with observations) suggesting that the actual increase in the O_3 burden over western Europe was even greater.

4.4. Surface CO and Ozone

[55] Finally the impact on composition at the surface resulting from the fire emissions is examined. Figure 13 shows the increase in model CO and O_3 at the surface, between runs A and D, which is greatest over western Europe on 22 July 2004 (see Figure 12). Increased surface CO and O_3 is seen over large regions of the Northern Hemisphere, and parts of the UK have model increases in CO and O_3 over 60 ppbv and 6 ppbv respectively. However, we noted earlier that the model simulations are consistent with considerable vertical mixing over the west coast of Europe, bringing tracers from the intense fire plume down to the surface. Measurements from the DLR Falcon indicate that much less vertical mixing of the plume occurred (Figures 5 and 8) so the model surface enhancements in CO and O_3 here are probably too large by a factor of two or more.

[56] Model results for surface CO and O_3 in the UK were compared to observations to look for any impacts on surface pollution from the fire emissions (Figure 14). Measurements of CO and O_3 were obtained from the Web site of the UK National Air Quality Information Archive. The hourly mean CO values from 16 coastal urban sites and O_3 values from 15 coastal or rural sites were obtained (to try to avoid local urban pollution). Diurnal minima in CO were used to look for enhancements in the background CO, but daytime diurnal maxima in O_3 were used to reduce the sensitivity to near-surface vertical mixing and emissions. These are compared to mean model values from runs A and D for the UK (in the region 7.0°W–1.4°E, and 50.4–58.8°N) at 1200 UT on each day. Measured CO is generally higher than in the model simulations probably because of the impact of local urban pollution, while measured O_3 is generally lower than in the model.

[57] The measurements show an enhancement in the background CO of about 20 ppbv on 22 and 23 July 2004, at the time that the intense fire plume was over western Europe. The increase in the model surface values of CO between runs A and D is greatest at about 56 ppbv on 21 and 22 July which coincides with the observations quite well. The low values in control run A at this time may be from the vertical mixing over the west coast of Europe bringing cleaner air down to the surface, and the high values in run D arise from the vertical mixing bringing down polluted air from the fire plume.

[58] The measurements do not show an obvious enhancement in background O_3 on 22 and 23 July, and there are only small increases in the model surface values of O_3 between runs A and D, greatest at about 6 ppbv on 21 and 22 July. Both model runs show enhanced O_3 for 21 to 23 July, probably from the vertical mixing over the west coast of Europe bringing down air from the upper troposphere. So, the observations possibly show increased background CO from the fire plume. However, finding a fire plume signal in the surface O_3 measurements is more difficult because of the much smaller enhancement expected.

5. Conclusions

[59] We have attempted to quantify the impact of the Alaskan and west Canadian wildfire emissions of summer 2004 on local, in-plume concentrations and on regional and hemispheric tropospheric ozone budgets. A series of model

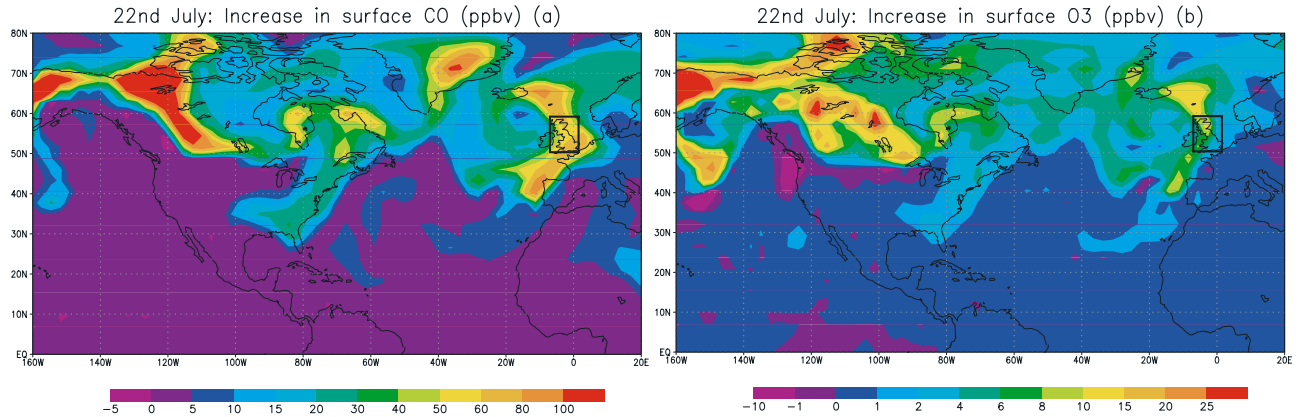

Figure 13. Increase in surface (a) CO and (b) O_3 (ppbv) on 22 July 2004 (1200 UT), difference between model runs A and D. The rectangle shows the area of the UK.

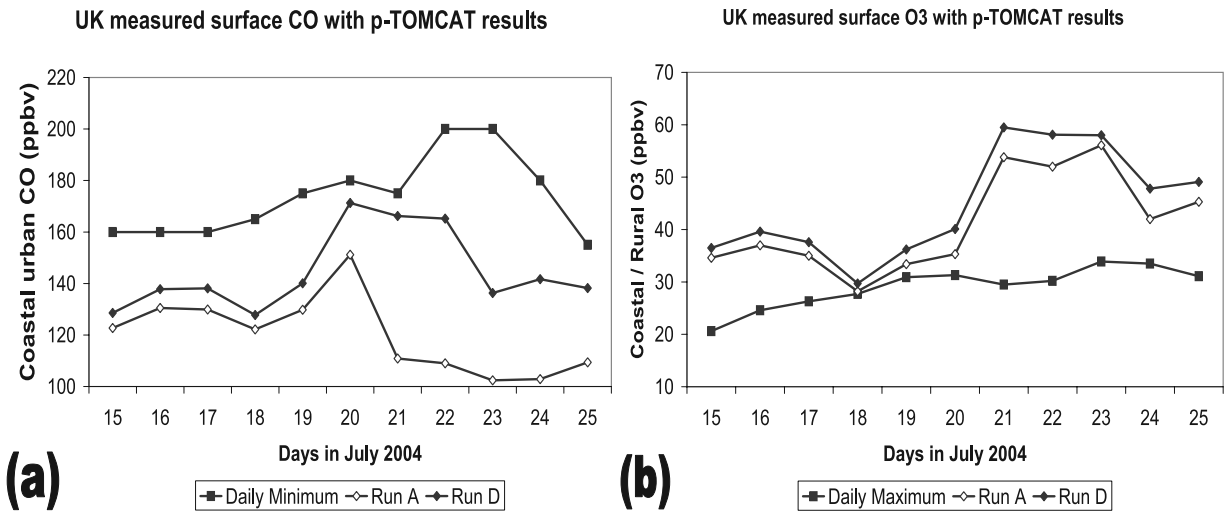

Figure 14. (a) Daily minimum surface measurements of CO (ppbv) (values from 16 coastal urban sites) and (b) daily maximum surface measurements of O_3 (ppbv) (values from 15 coastal and rural sites) from the UK during July 2004, with model values across the UK from runs A and D (the region covering 7.0°W–1.4°E, and 50.4–58.8°N) at 1200 UT on each day.

integrations has examined the effects of simple pyroconvective mixing of the ozone field over the fires, and of reducing the NO_2/CO emission ratio from the fires from 0.033 to 0.008, on both the ozone concentration within the observed fire plume and on the ozone budget. By using new inventories of biomass burning emissions during the period May to August 2004 in p-TOMCAT the CO plumes from the large forest fires in Alaska and west Canada can be reproduced in their location, altitude and magnitude. The model CO fields from simulations with the fire emissions have the same general pattern as the MOPITT satellite measurements, and closely match the measurements from the DC8 and BAe-146, although model convection is too vigorous over western Europe and agreement with the observed fire plumes breaks down there. These results lend strong support to the meteorology data used and to the locations and sizes of the CO sources in the new inventories.

[60] Model O_3 concentrations are initially too great within the plumes. Two sensitivity studies here have shown that the concentration can be substantially reduced, first, by applying additional vertical mixing of the tropospheric O_3 columns above the fires. There is evidence that considerable pyroconvective lofting of boundary layer air into the free troposphere took place above the fires. Secondly, O_3 in the model plume can be further reduced by decreasing the NO_2 emissions from the fires so that O_3 production is decreased, and measurements from the DC8 suggest that model NO_y is otherwise too great in the plume. Boreal fires are different from tropical fires in having lower NO_2/CO emission ratios and a rapid conversion of NO_x to PAN within the plumes [*Wofsy et al.*, 1992; *Bertschi et al.*, 2004]. Two possible explanations for the low NO_2/CO emission ratio from boreal fires are a greater prevalence of smoldering combustion in the fires and the lower nitrogen concentrations in boreal vegetation [*Wofsy et al.*, 1992]. Given the nature of these fires (very rapid combustion) the latter explanation seems the more likely but further research is needed on the NO_2/CO emission ratio from biomass burning, in particular because O_3 production depends critically on the NO_2/CO ratio [*McKeen et al.*, 2002]. By including the additional vertical mixing and decreasing the NO_2 emissions the NO_2 model field is closer to the SCIAMACHY satellite measurements, and the NO and O_3 in the model plumes is much closer to the measurements from the DC8 and the BAe-146.

[61] The model has been used to examine the impact of the fire emissions on O_3 production and budgets within large regions of the troposphere and over the whole Northern Hemisphere. The simulations indicate that the fire emissions lead to a significant increase in tropospheric O_3 during June to August 2004, with increases in production even over the Atlantic and western Europe. In the sensitivity study between model runs B and C the additional vertical mixing of O_3 above the fires reduces the peak increase in the Northern Hemisphere tropospheric O_3 burden by almost a third from 9.0 to 6.2 Tg. Then in the sensitivity study between runs C and D decreasing the NO_2 emissions from the fires reduces the peak increase in the tropospheric O_3 burden by a further two thirds to 2.0 Tg. Even this lower estimate is still 10% of projected increases in global ozone concentrations from 2000 to 2030 under a "current legislation" scenario. The large sensitivity of ozone production to the NO_2/CO ratio assumed in the biomass burning inventories shows that a single NO_2/CO ratio cannot be used for all types of wildfires and that there is a need to better quantify estimates of NO_2 emissions from biomass burning.

[62] Compared to the measurements of the fire plume by the DC8 and BAe-146 model runs B and C give too high NO, O_3 and NO_y and so overestimate the O_3 production, while model run D is much closer to the observed O_3 but has too little PAN, because of the lack of VOCs in the model chemistry, which would decompose downwind releasing further NO_x [*Hudman et al.*, 2004; *Real et al.*, 2007], and run D hence underestimates O_3 production. Therefore the model simulations suggest that the O_3 produced by the fire emissions in the Northern Hemisphere troposphere would have reached a peak between 2.0 Tg

(run D) and 6.2 Tg (run C) over a burden in run A of about 150 Tg (O_3). The model may also overestimate O_3 production because of the low spatial resolution smoothing out the NO_x field and the nonlinear relationship between NO_x concentration and O_3 production. For these reasons we regard the model sensitivity studies as providing lower and upper limits to the increase in O_3 from the Alaska and west Canada fire emissions.

[63] The impact of the fires may have been seen in the surface observations of background CO in the UK where both the model and observations show an increase of at least 20 ppbv on 22–23 July 2004. The modeled increase of O_3 at the surface is very small (a few ppbv) and is undetectable in the observations.

[64] **Acknowledgments.** We wish to thank the following: NERC for funding the ITOP Program, their support of NCAS-ACMSU and for supercomputer resources; Paul Young for further development of p-TOMCAT; Ronald C. Cohen and Jack E. Dibb for providing the NO_2 and HNO_3 data from the DC8; the NCAR MOPITT team for the CO satellite data; AEA Technology Environment and DEFRA for the data on the UK National Air Quality Information Archive web site; John Methven for providing the panels in Figure 1; and Oliver Wild for advice on the paper.

References

Aghedo, A. M., et al. (2006), The influence of African air pollution on regional and global tropospheric chemistry, *Atmos. Chem. Phys. Disc.*, *6*, 5797–5838.

Bertschi, I. T., et al. (2004), PHOBEA/ITCT 2002 airborne observations of transpacific transport of ozone, CO, volatile organic compounds, and aerosols to the northeast Pacific: Impacts of Asian anthropogenic and Siberian boreal fire emissions, *J. Geophys. Res.*, *109*, D23S12, doi:10.1029/2003JD004328.

Bovensmann, H., et al. (1999), SCIAMACHY—Mission objectives and measurement modes, *J. Atmos. Sci.*, *56*, 127–150.

Brough, N., et al. (2003), Intercomparison of aircraft instruments on board the C-130 and Falcon 20 over southern Germany during EXPORT 2000, *Atmos. Chem. Phys.*, *3*, 2127–2138.

Carver, G. D., and P. A. Stott (2000), IMPACT: An implicit time integration scheme for chemical species and families, *Ann. Geophys.*, *18*, 337–346.

Carver, G. D., P. D. Brown, and O. Wild (1997), The ASAD atmospheric chemistry integration package and chemical reaction database, *Comput. Phys. Commun.*, *105*, 197–215.

Chandra, S., et al. (2002), Tropical tropospheric ozone: Implications for dynamics and biomass burning, *J. Geophys. Res.*, *107*(D14), 4188, doi:10.1029/2001JD000447.

Chipperfield, M. P., et al. (1996), Analysis of UARS data in the southern polar vortex in September 1992 using a chemical transport model, *J. Geophys. Res.*, *101*, 18,861–18,881.

Cleary, P. A., P. J. Wooldridge, and R. C. Cohen (2002), Laser-induced fluorescence detection of atmospheric NO_2 with a commercial diode laser and a supersonic expansion, *Appl. Opt.*, *41*, 6950–6956.

Damoah, R., et al. (2006), A case study of pyroconvection using a transport model and remote sensing data, *Atmos. Chem. Phys.*, *6*, 173–185.

Drummond, J. R., and G. S. Mand (1996), The Measurement of Pollution in the Troposphere (MOPITT) instrument: Overall performance and calibration requirements, *J. Atmos. Oceanic Technol.*, *13*, 314–320.

Duncan, B. N., et al. (2003a), Interannual and seasonal variability of biomass burning emissions constrained by satellite observations, *J. Geophys. Res.*, *108*(D2), 4100, doi:10.1029/2002JD002378.

Duncan, B. N., et al. (2003b), Indonesian wildfires of 1997: Impact on tropospheric chemistry, *J. Geophys. Res.*, *108*(D15), 4458, doi:10.1029/2002JD003195.

Edwards, D. P., C. M. Halvorson, and J. C. Gille (1999), Radiative transfer modeling of the EOS Terra Satellite Measurement of Pollution in the Troposphere (MOPITT) instrument, *J. Geophys. Res.*, *104*, 16,755–16,775.

Fehsenfeld, F. C., et al. (2006), International Consortium for Atmospheric Research on Transport and Transformation (ICARTT): North America to Europe—Overview of the 2004 summer field study, *J. Geophys. Res.*, *111*, D23S01, doi:10.1029/2006JD007829.

Fromm, M., et al. (2005), Pyrocumulonimbus injection of smoke to the stratosphere: Observations and impact of the super blowup in northwestern Canada on 3–4 August 1998, *J. Geophys. Res.*, *110*, D08205, doi:10.1029/2004JD005350.

Gauss, M., et al. (2003), Radiative forcing in the 21st century due to ozone changes in the troposphere and the lower stratosphere, *J. Geophys. Res.*, *108*(D9), 4292, doi:10.1029/2002JD002624.

Gerbig, C. H., et al. (1999), An improved fast-response VUV resonance fluorescence CO instrument, *J. Geophys. Res.*, *104*, 1699–1704.

Giannakopoulos, C., et al. (1999), Validation and intercomparison of wet and dry deposition schemes using 210Pb in a global three-dimensional off-line chemical transport model, *J. Geophys. Res.*, *104*, 23,761–23,784.

Green, T. J., et al. (2006), An improved dual channel PERCA instrument for atmospheric measurements of peroxy radicals, *J. Environ. Monit.*, *8*, 530–536, doi:10.1039/b514630e.

Hao, W. M., and M. H. Liu (1994), Spatial and temporal distribution of tropical biomass burning, *Global Biogeochem. Cycles*, *8*, 495–503.

Holtslag, A. A. M., and B. A. Boville (1993), Local versus nonlocal boundary-layer diffusion in a global climate model, *J. Clim.*, *6*(10), 1825–1842.

Hudman, R. C., et al. (2004), Ozone production in transpacific Asian pollution plumes and implications for ozone air quality in California, *J. Geophys. Res.*, *109*, D23S10, doi:10.1029/2004JD004974.

Law, K. S., and E. G. Nisbet (1996), Sensitivity of the methane growth rate to changes in methane emissions from natural gas and coal, *J. Geophys. Res.*, *101*, 14,387–14,397.

Law, K. S., et al. (1998), Evaluation of modeled O_3 using MOZAIC data, *J. Geophys. Res.*, *103*, 25,721–25,737.

Law, K. S., et al. (2000), Comparison between global chemistry transport model results and Measurement of Ozone and Water Vapor by Airbus In-Service Aircraft (MOZAIC) data, *J. Geophys. Res.*, *105*, 1503–1525.

McKeen, S. A., et al. (2002), Ozone production from Canadian wildfires during June and July of 1995, *J. Geophys. Res.*, *107*(D14), 4192, doi:10.1029/2001JD000697.

Methven, J., S. R. Arnold, F. M. O'Connor, H. Barjat, K. Dewey, J. Kent, and N. Brough (2003), Estimating photochemically produced ozone throughout a domain using flight data and a Lagrangian model, *J. Geophys. Res.*, *108*(D9), 4271, doi:10.1029/2002JD002955.

Methven, J., et al. (2006), Establishing Lagrangian connections between observations within air masses crossing the Atlantic during the International Consortium for Atmospheric Research on Transport and Transformation experiment, *J. Geophys. Res.*, *111*, D23S62, doi:10.1029/2006JD007540.

O'Connor, F. M., et al. (2004), Tropospheric ozone budget: Regional and global calculations, *Atmos. Chem. Phys. Disc.*, *4*, 991–1036.

O'Connor, F. M., et al. (2005), Comparison and visualisation of high-resolution transport modeling with aircraft measurements, *Atmos. Sci. Lett.*, *6*, 164–170, doi:10.1002/asl.111.

Pfister, G., et al. (2005), Quantifying CO emissions from the 2004 Alaskan wildfires using MOPITT CO data, *Geophys. Res. Lett.*, *32*, L11809, doi:10.1029/2005GL022995.

Prather, M. J. (1986), Numerical advection by conservation of second-order moments, *J. Geophys. Res.*, *91*, 6671–6681.

Price, C., and D. Rind (1992), A simple lightning parameterization for calculating global lightning distributions, *J. Geophys. Res.*, *97*, 9919–9933.

Real, E., et al. (2007), Processes influencing ozone levels in Alaskan forest fire plumes during long-range transport over the North Atlantic, *J. Geophys. Res.*, doi:10.1029/2006JD007576, in press.

Richter, A., and J. P. Burrows (2002), Retrieval of tropospheric NO_2 from GOME measurements, *Adv. Space Res.*, *29*, 1673–1683.

Richter, A., et al. (2005), Increase in tropospheric nitrogen dioxide over China observed from space, *Nature*, *437*, 129–132, doi:10.1038/nature04092.

Savage, N. H., et al. (2004), Using GOME NO_2 satellite data to examine regional differences in TOMCAT model performance, *Atmos. Chem. Phys.*, *4*, 1895–1912.

Schlager, H., et al. (1999), Regional nitric oxide enhancements in the North Atlantic flight corridor observed and modeled during POLINAT 2: A case study, *Geophys. Res. Lett.*, *26*, 3061–3064.

Singh, H. B., W. H. Brune, J. H. Crawford, D. J. Jacob, and P. B. Russell (2006), Overview of the summer 2 004 Intercontinental Chemical Transport Experiment–North America (INTEX-A), *J. Geophys. Res.*, *111*, D24S01, doi:10.1029/2006JD007905.

Stevenson, D. S., et al. (2006), Multimodel ensemble simulations of present-day and near-future tropospheric ozone, *J. Geophys. Res.*, *111*, D08301, doi:10.1029/2005JD006338.

Stockwell, D. Z., et al. (1999), Modelling NO_x from lightning and its impact on global chemical fields, *Atmos. Environ.*, *33*, 4477–4493.

Tiedke, M. (1989), A comprehensive mass flux scheme for cumulus parameterization in large-scale models, *Mon. Weather Rev.*, *117*, 1779–1800.

Turquety, S., et al. (2007), Inventory of boreal fire emissions for North America in 2004: Importance of peat burning and pyroconvective injection, *J. Geophys. Res.*, *112*, D12S03, doi:10.1029/2006JD007281.

Wang, K. Y., J. A. Pyle, and C. Bridgeman (1999), Implementation of a convective atmospheric boundary layer scheme in a tropospheric chemistry transport model, *J. Geophys. Res.*, *104*, 23,729–23,745.

Whalley, L. K., et al. (2004), Two high-speed, portable GC systems designed for the measurement of non-methane hydrocarbons and PAN: Results from the Jungfraujoch High Altitude Observatory, *J. Environ. Monit.*, *6*, 234–241.

Wild, O., et al. (1996), Photochemical trajectory modeling studies of the North Atlantic region during August 1993, *J. Geophys. Res.*, *101*, 29,269–29,288.

Wofsy, S. C., et al. (1992), Atmospheric chemistry in the Arctic and subarctic: Influence of natural fires, industrial emissions, and stratospheric inputs, *J. Geophys. Res.*, *97*, 16,731–16,746.

Wotawa, G., and M. Trainer (2000), The influence of Canadian forest fires on pollutant concentrations in the United States, *Science*, *288*, 324–328.

Yevich, R., and J. A. Logan (2003), An assessment of biofuel use and burning of agricultural waste in the developing world, *Global Biogeochem. Cycles*, *17*(4), 1095, doi:10.1029/2002GB001952.

M. A. Avery and G. W. Sachse, NASA Langley Research Center, Hampton, VA 23681, USA.

W. Brune, Department of Meteorology, Pennsylvania State University, University Park, PA 16802, USA.

J. P. Burrows, A. Heckel, and A. Richter, Institute of Environmental Physics, University of Bremen, D-28359 Bremen, Germany.

G. D. Carver, P. A. Cook, J. G. Levine, and J. A. Pyle, Centre for Atmospheric Science, Department of Chemistry, University of Cambridge, Cambridge CB2 1EW, UK. (john.pyle@atm.ch.cam.ac.uk)

A. C. Lewis, Department of Chemistry, University of York, York YO10 5DD, UK.

P. S. Monks and A. E. Parker, Department of Chemistry, University of Leicester, Leicester LE1 7RH, UK.

F. M. O'Connor and N. H. Savage, Met Office, Exeter EX1 3PB, UK.

R. Purvis, Facility of Airborne Atmospheric Measurements, Cranfield MK43 0AL, UK.

C. E. Reeves and D. Stewart, School of Environmental Sciences, University of East Anglia, Norwich NR4 7TJ, UK.

H. Schlager, Institut fuer Physik der Atmosphaere, Deutsches Zentrum fuer Luft- und Raumfahrt, D-82230 Oberpfaffenhofen, Germany.

H. B. Singh, NASA Ames Research Center, Moffett Field, CA 94035, USA.

S. Turquety, Service d'Aéronomie, Institut Pierre-Simon Laplace, F-75005 Paris, France.

L. K. Whalley, School of Chemistry, University of Leeds, Leeds LS2 9JT, UK.